TU/e Technische Universiteit
Eindhoven
University of Technology

Department of Mechanical Engineering
Dynamics & Control

Influence of different road surface types on tyre turn slip & friction characteristics

Internship Report
DC2016.098

Rohan Lakhotia

Supervisors:
Ir. Carlo Lugaro (TASS International)
Dr. Ir. Igo Besselink (Eindhoven University of Technology)
Prof. Dr. Henk Nijmeijer (Eindhoven University of Technology)

Eindhoven, Friday 27th January, 2017

Summary

This project was done at TASS International, Helmond to investigate the influence of different road surfaces on tyre turn slip and their friction characteristics. It has been observed that there is a difference in the peak aligning moment predicted by the MF-Tyre/MF-Swift model with respect to the measured data. This is most likely caused due to different parameters used by the MF-Tyre/MF-Swift model as compared to the test surface used during measurements.

This report investigates the influence of different road surfaces on the aligning moment generated during turn-slip measurements. Three different tyres compounds are used for the measurements at different operating conditions such as the inflation pressure and applied vertical force. The measurements are performed at a constant steering rate at standstill conditions and on five different test surfaces.

The measurements are then analysed and we try to investigate the effect of the different surfaces on the self aligning moment generated by the tyres during turn slip.

Preface

This report describes the project done at TASS International, Helmond for my internship. TASS International supports the vehicle industry by providing software products such as Delft-Tyre, PreScan and MADYMO. The Delft-Tyre product is based on the renown Magic Formula and has been extended to become an accurate and quick modelling tool for tyres. The aim of this internship is to understand the effect of surface friction on a standstill parking manoeuvre.

This report discusses rubber friction and the hysteretic friction theory introduced by Persson. The second half of the report is a discussion on the measurements, which were done using the Flat Plank tyre tester, at Eindhoven University of Technology. Finally, some conclusions are discussed and recommendations for the topic are made.

Acknowledgement

I would like to thank TASS International for providing me the opportunity to do my internship with them. It has truly been a learning experience, especially in the field of tyre modelling.

I would like to take this opportunity to thank my project supervisor, Carlo Lugaro for his guidance and support during this project and Willem Versteden for giving me the opportunity to work on this project. Furthermore, I thank my colleagues at TASS International for their support during the course of this internship.

I am grateful to Erwin Meinders from the AES lab of the Eindhoven University of Technology for helping me to acquire the different road surfaces and to Jeroen Brouwer for helping me understand how to operate the Flat Plank tyre tester.

Finally, I would like to thank Dr. Ir. Igo Besselink and Prof. Dr. Henk Nijmeijer for their support and guidance throughout this project.

Abbreviations

ADAS	Advanced driver assistance systems
DAB	Dicht Asfaltbeton/ Closed asphalt
EPS	Electric power steering
Tyre 1	Continental ContiEcoContact 5 175/65R14
Tyre 2	Bridgestone Potenza RE050A 175/55R15
Tyre 3	Continental ContiWinterContact TS850 205/55R17
ZOAB	Zeer open asfaltbeton/ Open asphalt

Symbols

a	Half of contact patch length $[m]$
α	Slip angle $[deg]$
b	Half of contact patch width $[m]$
β	Tyre yaw torsion angle $[deg]$
$C_{M\alpha}$	Aligning stiffness $[Nm/deg]$
$C_{M\psi}$	Yaw stiffness $[Nm/rad]$
$C(q)$	Surface power spectrum $[m^4]$
$E(w)$	Complex tensile modulus of rubber $[Nm^{-2}]$
F_z	Vertical force $[N]$
$G(\omega)$	Complex shear modulus $[Nm^{-2}]$
μ	Friction coefficient $[-]$
M_z	Aligning moment $[Nm]$
$M_{z,peak}$	Peak aligning moment $[Nm]$
ν	Poisson ratio for rubber $[-]$
$P(q)$	Ratio of actual contact area to nominal contact area $[-]$
ψ	Yaw angle $[deg]$
q	Wavenumber $[-]$
σ_z	Nominal stress $[Nm^{-2}]$
v	Sliding velocity $[ms^{-1}]$
ω_{LMP}	Frequency where rubber has its loss modulo peak $[Hz]$

Contents

Chapter 1

Introduction

Tyre models are an essential tool in the automotive and aviation industry. For the development of cars and advanced driver assistance systems (ADAS), computer models are required to predict the response of the system accurately. For the driver assist systems, such as electric power steering (EPS) and assisted parking systems, it is important to accurately predict the forces and moments generated by the tyre. Turn slip has recently been incorporated in the Pacejka Magic Formula model [6]. This has been developed further and included in the MF-Tyre/MF-Swift-6.2 model [10]. This extension is used to identify the forces and moments generated by the tyre when steered at a low speed or standstill conditions [6]. To define the characteristics of the turn slip model, a set of parameters need to be defined. These parameters are dependent on the operating conditions, such as the tyre's inflation pressure, vertical force, surface roughness, etc.

The MF-Tyre/MF-Swift model has been extended to include inflation pressure changes [8]. Surface roughness also influences the frictional characteristics between the tyre and road surface. It has been observed in [4], that there is a difference in the peak aligning moment ($M_{z,peak}$) predicted by the model and the measured data for parking manoeuvres. This difference is most likely caused by a different coefficient of friction (μ) used for the parameter identification compared to the actual test surface on which the measurements were executed. This study is done to investigate the influence of different road surface types on tyre turn slip and friction characteristics. Based on the results, we aim to define scaling parameters to account for different surface roughness based on contact mechanics.

Chapter 2 explains Persson's hysteresis theory and it's application to rubber-road surface friction. Chapter 3 discusses the MF-Tyre/MF-Swift model and it's extensions to include turn slip. The Van der Jagt model for non-rolling tyres for standstill parking measurements will be described. Chapter 4 discusses the measurement setup and the operating conditions. The measurement data is then analysed in the same chapter.

Chapter 2

Rubber friction on road surfaces

2.1 Introduction

It is important to understand the interaction between the road surface and the rubber tyre. The friction depends on various factors such as the applied vertical force, surface properties, temperature and sliding velocity. For road surfaces, the rubber friction arises from the time dependent viscoelastic deformations of the rubber by the substrate properties [3]. We will investigate the various factors that affect the friction between the substrate and the surface.

Section 2.2 gives a brief explanation on rubber friction. Persson's Hysteresis theory is discussed in section 2.3.

2.2 Rubber friction

Compared to other solids, rubber friction has different frictional properties. This is because of the rubber's low elastic modulus and it's high internal friction. The frictional force between rubber and a rough surface are a result of adhesion and hysteretic components [5]. The hysteretic component is due to to the internal friction of the rubber. The asperities of the rough surface exert oscillating forces on the rubber surface during sliding. This leads to deformation of the rubber and energy dissipation because of the internal damping of the rubber. The adhesive forces are more important for clean and relatively smooth surfaces [7]. The components of rubber friction can be explained by decomposing it into elementary mechanisms shown in figure 2.1. Four components of rubber friction can be distinguished:

  i Hysteresis energy loss due to damping of surface-induced vibrations inside the rubber. Hysteresis energy loss is the most important component when studying rubber friction on rough road surfaces.

 ii Adhesion friction. This component is a result of the physical bond between the two bodies when in close contact.

iii Viscous friction with the medium which is confined between the rubber and road surface, eg. when sliding over a water film.

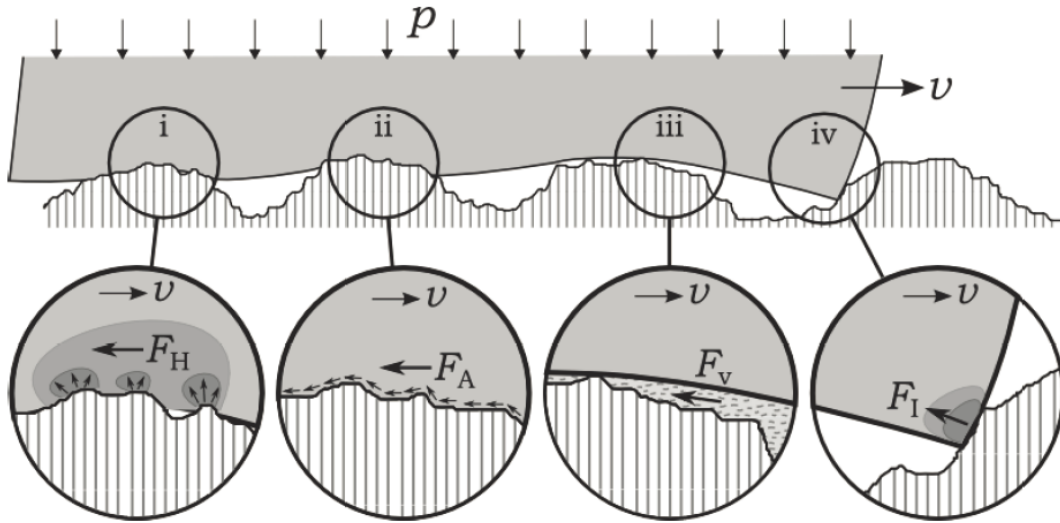 iv Resistive forces due to mechanical interlocking of the rubber with the surface.

Figure 2.1: Rubber block sliding on a rough surface [2]

2.3 Persson's Hysteresis Theory

The rubber and road surface interaction can be considered by assuming the road surface to be a simple sinusoidal profile. This is later extended to a combination of multiple wavelengths, as shown in figure 2.2.
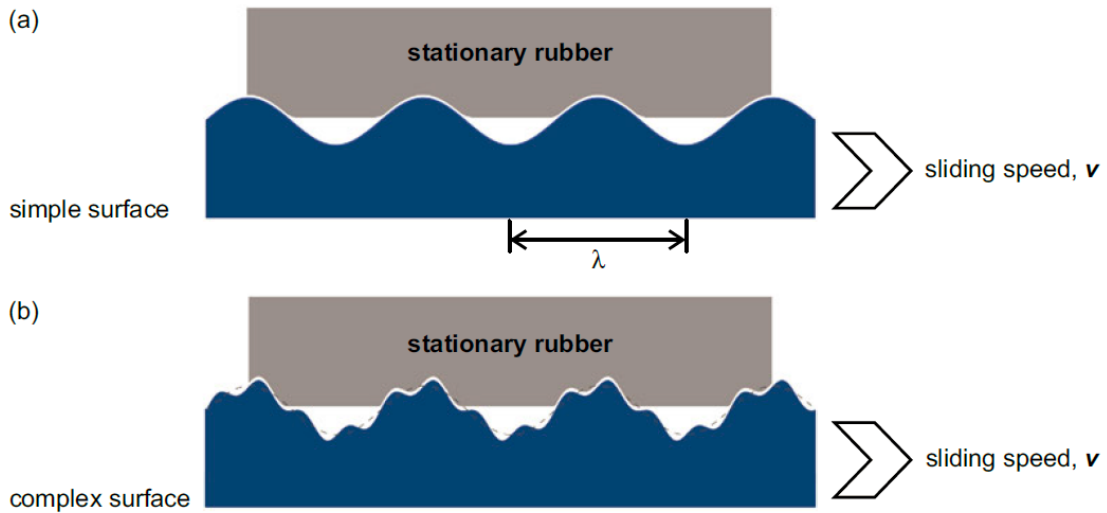

Figure 2.2: Representation of interaction between rubber block and surface. [9]

The rubber's conformation to the rigid surface depends on the normal force and stiffness of the rubber. In the more complex case, the conformity of the rubber over short wave irregularities depends on the presence of long wavelengths, which affect the normal loading between surfaces.

When the surface is sinusoidal, the energy dissipation would be maximal when the sliding

velocity is such that deformation frequency equals ω_{LMP}, (Loss Modulo Peak) [9]. Based on this and according to Persson's deformation theory [7], the peak friction for a particular sliding velocity (v) equals:

$$\mu = \frac{1}{2} \int_{q_0}^{q_1} q^3 C(q) P(q) dq. \int_0^{2\pi} \cos(\phi) \operatorname{Im}\left(\frac{2G(qv\cos(\phi), T)}{\sigma_z(1-\nu)}\right) d\phi \tag{2.1}$$

Where, $C(q)$ is the surface power spectrum, $P(q)$ is the ratio of real contact area to nominal contact area. The nominal contact area corresponds to a complete filling of all surface voids by the rubber. T is the rubber's temperature. $G(\omega)$ is the complex shear modulus of the rubber compound and is related to the tensile modulus $E(w)$ by:

$$E(\omega) = 2(1+\nu)G(\omega) \tag{2.2}$$

The frequency dependency of $G(\omega)$ is expressed in terms of it's sliding velocity (v) as:

$$\omega = qv\cos(\phi) \tag{2.3}$$

Where, ϕ is the angle between the sliding direction and orientations of the road undulations, described by wavenumber q. σ_z is the normal pressure applied to the tyre and ν is the Poisson ratio of the rubber compound.

Under the normal vertical stress σ_z the surface asperities do not fully penetrate the rubber. Only a partial contact between the surface and the rubber block happens. So, the power spectrum does not completely contribute to the hysteretic friction. This is implemented in equation (2.1) by using $P(q)$.

$$P(q) = \frac{2}{\pi} \int_0^\infty \frac{\sin(x)}{x} e^{-x^2 F(q)} dx \tag{2.4}$$

Where,

$$F(q) = \frac{1}{8} \int_{q_0}^{q_1} q^3 C(q) dq \int_0^{2\pi} \left|\frac{2(1+\nu)G(qv\cos(\phi), T)}{(1-\nu^2)\sigma_z}\right|^2 \tag{2.5}$$

When $\sigma_z \ll G(0)$, where $G(0)$ equals the rubber compound's static shear stiffness, then $P(q)$ can be approximated by [7]:

$$P(q) = \left[\frac{\pi}{8} \int_{q_0}^{q_1} q^3 C(q) dq \int_0^{2\pi} \left|\frac{2G(qv\cos(\phi), T)}{(1-\nu)\sigma_z}\right|^2 d\phi\right]^{-1/2} \tag{2.6}$$

From equation (2.6), it is observed that the normalized contact area $P(q)$ is directly proportional to σ_z and inversely proportional to the rubber compound's stiffness.

2.4 Application of Persson's theory

As discussed in section 2.3, the tyre's complex shear modulus $G(qv\cos(\phi))$ and the surface vertical displacement power spectral density $C(q)$ is required to quantitatively predict the hysteretic friction component.

However, the complex shear modulus of rubber tyres is not generally available. Measuring this quantity is out of the scope of this project. The surface vertical displacement power spectral density $C(q)$ can be obtained using a surface profiler. Sensofar PLμ2300 Optical Surface Profiler from the Multi-scale lab at TU/e can be used to obtain $C(q)$.

Since, limited data is available to do a detailed microscopic analysis, the research focusses on the overall macroscopic charachteristics obtained for a tyre in this project. The results will be used to develop a method to scale the peak friction values for different road surfaces.

Chapter 3

The MF-Tyre/MF-Swift Model

3.1 Introduction

The MF-Tyre/MF-Swift model is one of the most used tyre models worldwide. It has been widely accepted as an accurate model used to describe the forces and moments developed by a rolling tyre under various slip conditions [8].

The extensions to the Magic Formula for turn slip will be discussed in section 3.2. The Van der Jagt parking model extension for a non-rolling tyre will be described in section 3.3.

3.2 Extensions of the Magic Formula

The contribution of turn slip has been introduced in the Pacejka Magic Formula model [6] and has been incorporated in the MF-Tyre/MF-Swift software by [10]. The extensions are [4]:

1. Adaptations on the Magic formula to describe the forces and moments generated by a rolling tyre, when spin (turn slip) is an additional input [6].

2. A model that can predict the aligning moment generated by a non-rolling tyre. The Van der Jagt model is used as a reference for this [1].

3. A transition model, which depends on the forward speed can switch between equations for the rolling non-rolling tyre [6].

3.3 Non-rolling tyre model

At standstill, the tyre reduces to a spring with stiffness $C_{M\psi}$. However, this is only valid when the contact patch is in adhesion (small steering inputs). For larger steering inputs the tyre slides and the aligning moment (M_z) generated by the tyre increases in a non-linear way until the friction limit is reached [4]. The Van der Jagt model [1] can describe this behaviour. This model consists of the following equations:

$$\begin{cases} \dot{\beta} = -\left(1 - p\left|\frac{M_z}{M_{z\varphi\infty}}\right|^{c_0}\right)\dot{\psi} \\ M_z = C_{M\psi}\beta \\ if\left((sign(\beta) \neq -sign(\dot{\psi})\right)\ p = 0\ else\ p = 1 \end{cases} \tag{3.1}$$

Where, β is the tyre torsion angle, ψ is the yaw angle and $C_{M\psi}$ is the yaw stiffness of the tyre. From equation (3.1), when $p = 0$ or $M_z = 0$, the gradient of M_z gives:

$$\left.\frac{\partial M_z}{\partial \psi}\right|_{p=0} = -C_{M\psi} \tag{3.2}$$

And for large steering angles:

$$M_z|_{\psi \to \pm\infty} = \mp M_{z\varphi\infty} \tag{3.3}$$

Equation (3.2) indicates that for small values of yaw angle (ψ), the tyre behaves like a torsional spring. For larger values, the M_z goes to the maximum value $M_{z\varphi\infty}$ that can be achieved when full sliding occurs. This transition is controlled by the exponent c_0.

Chapter 4

Measurements

4.1 Introduction

The aligning moment generated by a number of selected tyres was measured on the Flat plank tyre tester of the Eindhoven University of Technology. The measurements were done for five different road surfaces.

A brief overview of the Flat Plank tyre tester is given in section 4.2. The road surfaces used for the experiments are described in section 4.3. Section 4.4 discusses the choice of tyres used for the experiments. The measurement plan is discussed in section 4.5.

4.2 The Flat plank tyre tester

The standstill parking measurements were done using the Flat Plank tyre tester. This machine can be used for measurements up to a speed of 2.3 cm/s [6]. The wheel axle is equipped with a measuring hub, which can be steered, cambered and braked. Along the vertical axis, the vertical tyre force can be adjusted to the desired load. An impression of the Flat Plank tyre tester is shown in figure 4.1 [6]. The Flat Plank tyre tester was used since different road surfaces patches can be installed and used to evaluate tyre performance on different road surfaces.
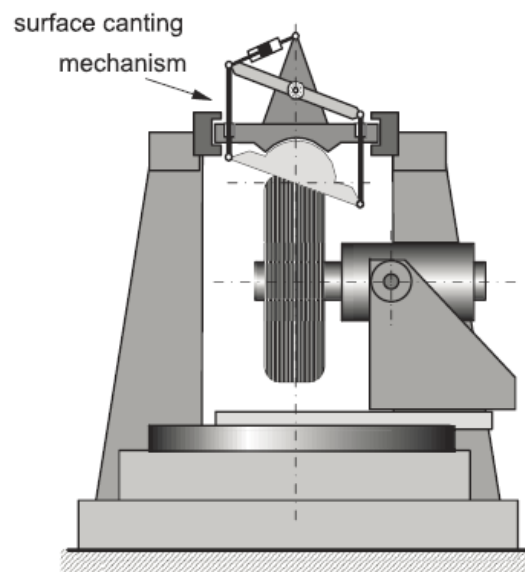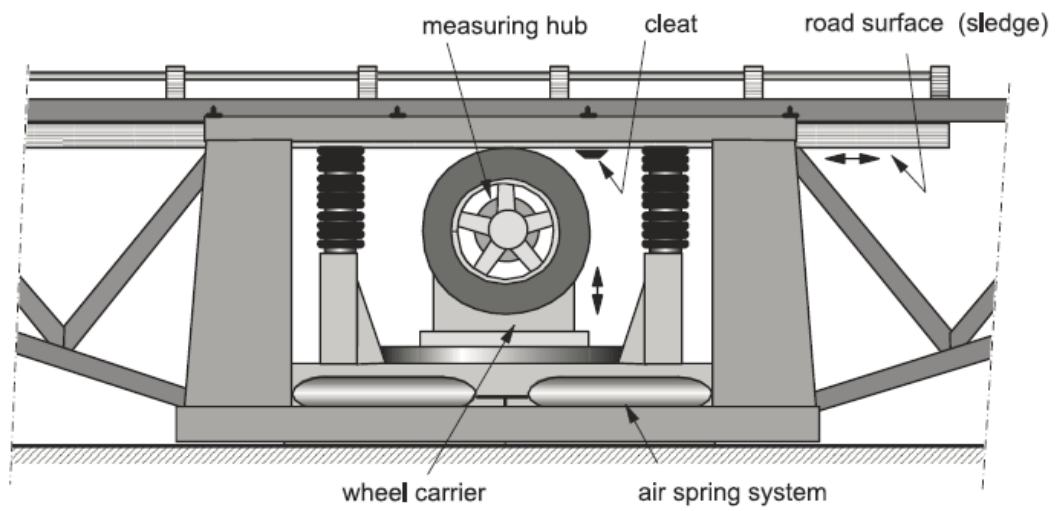
Figure 4.1: Flat plank tyre tester [6]

4.3 Surfaces

As discussed earlier in section 2.3, it is observed that the peak hysteretic friction is dependent on $C(q)$, the surface vertical displacement power spectral density. So, it was decided to perform measurements on different surfaces. The following surfaces were used:

1. Smooth surface of the flat plank.

2. "Safety-walk" (Sandpaper).

3. Beton: Concrete

4. DAB: Dicht asfaltbeton (Non porous/ Closed asphalt)

5. ZOAB: Zeer open asfaltbeton (Open/porous asphalt)

The Beton road surface is constructed in two layers, with the top layer brushed for increased friction. If not drained properly, it is prone to crack formation. It is often used for bus lanes.

The DAB road surface is dense asphalt and is non porous. It has high durability, however is known to have poor water drainage capabilities. It is cheap to construct and is used as the reference road surface when noise levels are compared.

The ZOAB road surface is open asphalt and is porous. It has low durability as compared to DAB road surface, but has superior drainage capabilities and hence used on motorways. It has a reduced tyre noise while driving when compared to the DAB road surface.

4.4 Tyre selection

For the measurements, three tyres were selected from a list of available tyres. Each tyre was of a different compound and size. It was decided to measure an eco tyre, a regular tyre and a winter tyre. The following tyres were selected:

- **Tyre 1**: Continental ContiEcoContact 5:

The Continental ContiEcoContact 5 175/65R14 (Tyre 1) has a maximum load rating of 530 kg and maximum inflation pressure of 350 kPa. The characteristics of Tyre 1 are given in table 4.1

Table 4.1: Tyre 1 parameters

Section Width	175 mm
Aspect Ratio	65
Construction	Radial
Rim Diameter	14 inch
Maximum Load	530 kg
Maximum Inflation Pressure	350 kPa

- **Tyre 2**: Bridgestone Potenza RE050A:

The Bridgestone Potenza RE050A 175/55R15 (Tyre 2) has a maximum load rating of 412 kg and maximum inflation pressure of 350 kPa. The characteristics of Tyre 2 are given in table 4.2

Table 4.2: Tyre 2 parameters

Section Width	175 mm
Aspect Ratio	55
Construction	Radial
Rim Diameter	15 inch
Maximum Load	412 kg
Maximum Inflation Pressure	350 kPa

- **Tyre 3**: Continental ContiWinterContact TS850:

  The Continental ContiWinterContact TS850 205/55R17 (Tyre 3) has a maximum load rating of 615 kg and maximum inflation pressure of 300 kPa. The characteristics of Tyre 3 are given in table 4.3

Table 4.3: Tyre 3 parameters

Section Width	205 mm
Aspect Ratio	55
Construction	Radial
Rim Diameter	17 inch
Maximum Load	615 kg
Maximum Inflation Pressure	300 kPa

4.5 Measurement Plan

For the turn slip measurements, a number of inflation pressures and vertical forces were chosen based on each tyres maximum load index and permissible inflation pressure. They are listed in table 4.4.

Table 4.4: Vertical force and inflation pressure

	Vertical force [N]	Inflation pressure [kPa]
Tyre 1	[3000, 4000, 5000]	[200, 240, 280]
Tyre 2	[2000, 3000, 4000]	[200, 240, 280]
Tyre 3	[3500, 4500, 5500]	[180, 210, 240]

Typically a parking manoeuvre is a combination of standstill and rolling conditions. The manoeuvre starts from standstill and switches to driving at low speed, while steering the front wheels to large angles. The steering is done both at standstill and for rolling conditions.

If the driver accelerates and brakes the car in a gentle manner, then the longitudinal acceleration is low and hence the following assumptions are valid [4]:

1. Vertical force on the tyre is close to static conditions.

2. Longitudinal slip is zero.

For this study, focus is put on the self aligning moment (M_z) which is generated during turn slip at standstill conditions. For the measurement of M_z during turn slip, initially it was decided to observe the effect of different steering velocities on the moment generated. However, the flat plank could not handle high speeds, so a fixed steering rate of 1 deg/s was chosen. The wheel is steered to a maximum angle of 30 degrees and then to opposite steering angle of -30 degrees. This cycle is again repeated and then stopped at a steering abgle of 0 degrees, as shown in figure 4.2.
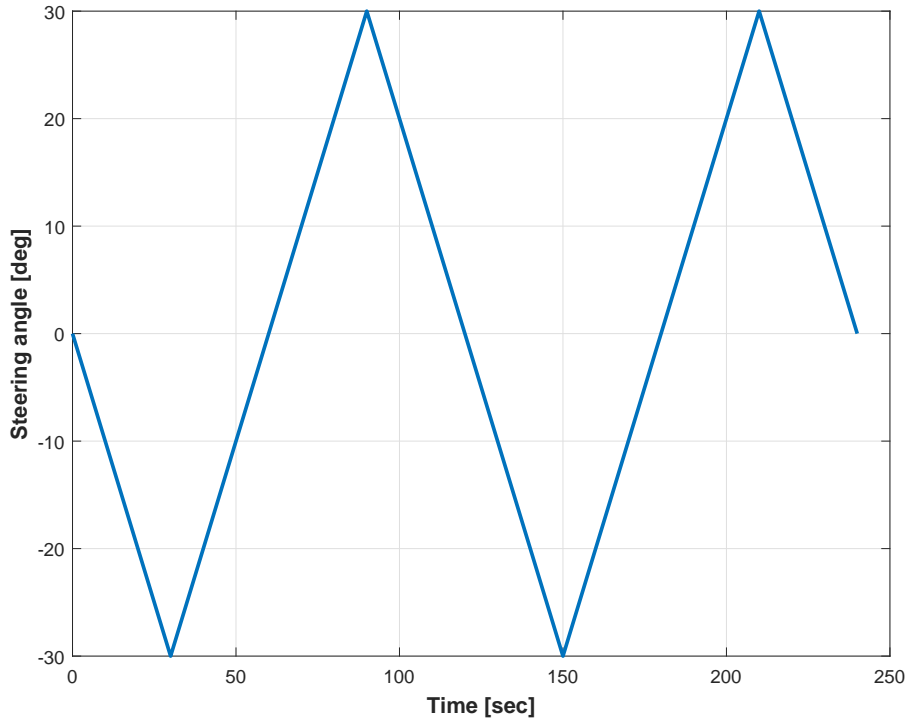
Figure 4.2: Steering angle input

The measurements were performed on the five road surfaces as mentioned in section 4.3. The following remarks can be made with respect to the road surfaces:

1. The sandpaper was not new. Measurements had been performed on it previously.

2. As the measurements were performed on the DAB and Beton surface, rubber from the tyre compound began to accumulate on the surface.

3. The ZOAB surface was heavily damaged after measuring the 1st tyre. Therefore the measurements on the ZOAB surface may be unreliable.

4. The Beton surface was brushed along the direction of motion instead of being perpendicular to the direction of motion.

4.6   Self aligning moment

The self aligning moment (M_z) was measured for the different operating conditions as defined in section 4.5. Self aligning moment (M_z) vs yaw angle (ψ) at nominal force and inflation pressure for Tyre 1 can be seen in figure 4.3, for Tyre 2 in figure 4.4 and Tyre 3 in figure 4.5.
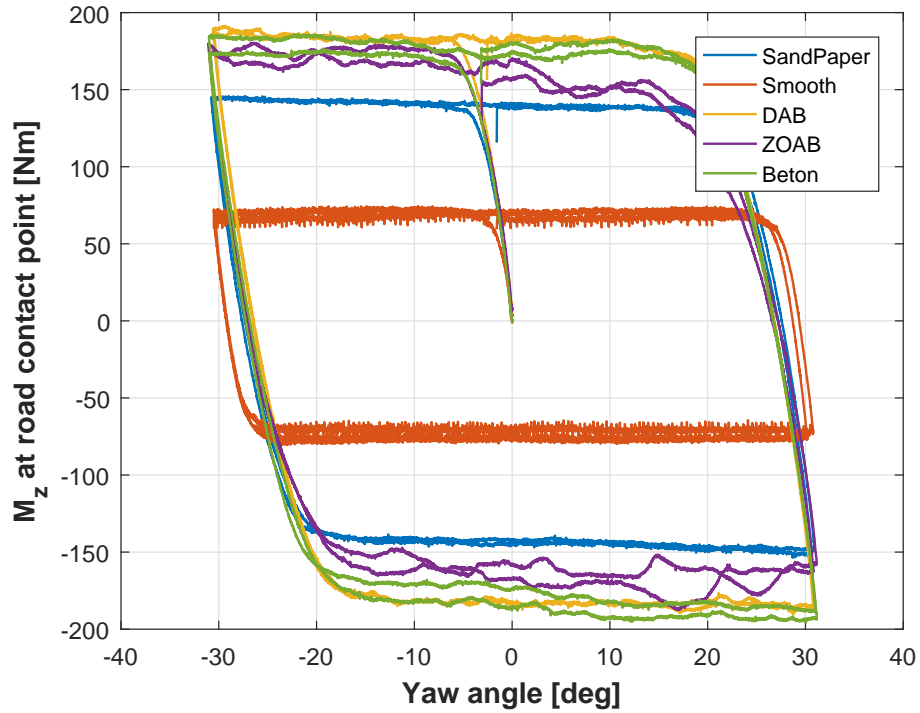
Figure 4.3: Tyre 1 M_z vs ψ (Inflation pressure: 240 kPa, Vertical force: 4000 N)
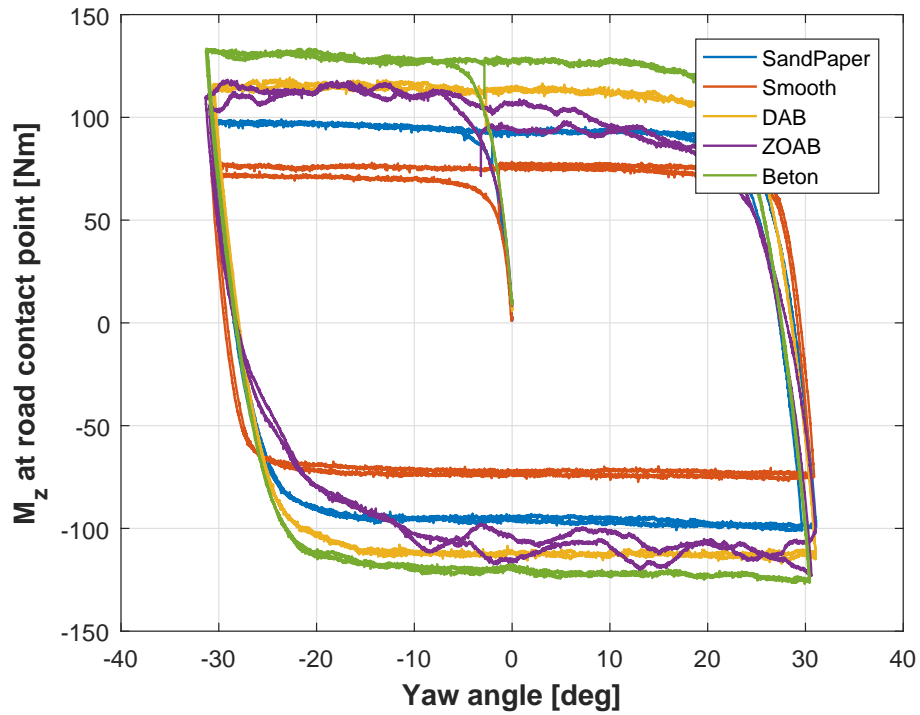
Figure 4.4: Tyre 2 M_z vs ψ (Inflation pressure: 240 kPa, Vertical force: 3000 N)
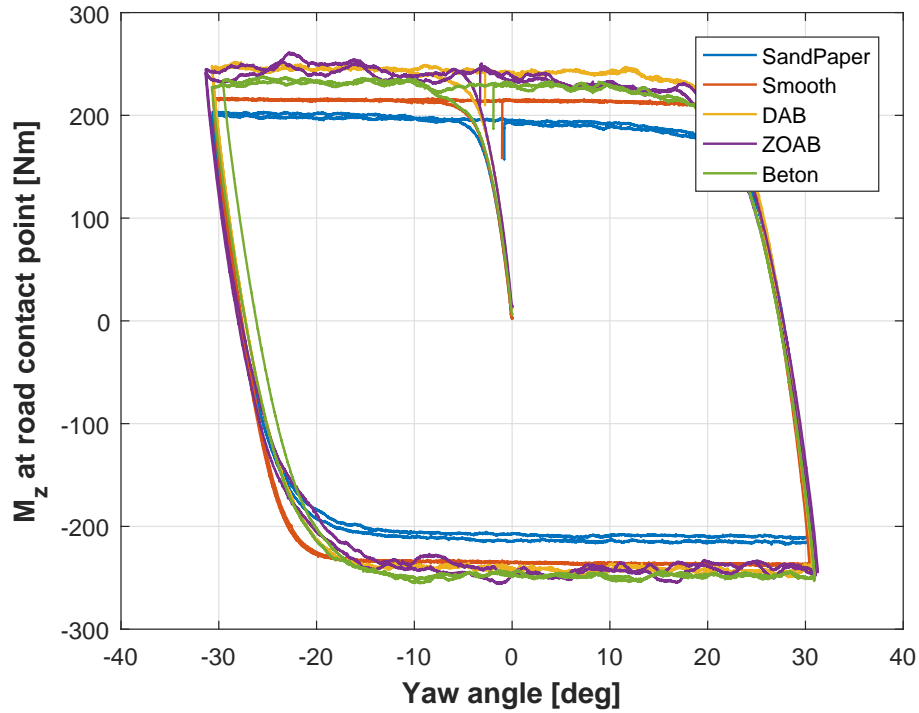
Figure 4.5: Tyre 3 M_z vs ψ (Inflation pressure: 210 kPa, Vertical force: 4500 N)

A noticeable difference from the graphs are observed in the self aligning moments due to the different surface properties. It can also be seen that different trends are observed depending on the tyre. This is because of the difference in the $E(w)$ values of each tyre, which would affect the peak hysteretic friction based on Persson's hysteresis theory [7]. From the measurements, it is evident that we need to analyse the surface roughness and the tyre properties to better understand the friction force generation. It was decided to compare the peak friction for different operating conditions. This will be be described in chapter 5. The measurements for the three tyres at different operating conditions can be seen in appendix A.

Chapter 5

Measurements Results

5.1 Introduction

After the measurements were completed on the Flat plank tyre tester, they were processed and analysed. The aligning stiffness, maximum aligning moment generated, contact patch dimensions and the peak frictions are estimated for the three tyres.

The peak aligning moment ($M_{z,peak}$) has been discussed in section 5.2. Then, the aligning stiffness ($C_{M\alpha}$) has been evaluated in section 5.3. The contact patch dimensions are measured in 5.4 and the peak friction coefficients are estimated in section 5.5.

5.2 Peak aligning moment

The peak aligning moment ($M_{z,peak}$) generated by the tyres are observed. It is observed that as the inflation pressure increases, the aligning moment generated by the tyre reduces. As expected, the $M_{z,peak}$ increases as the applied vertical force (F_z) increases. These can be seen in figures 5.1 and 5.2 for Tyre 1, figures 5.3 and 5.4 for Tyre 2 and figures 5.5 and 5.6 for Tyre 3
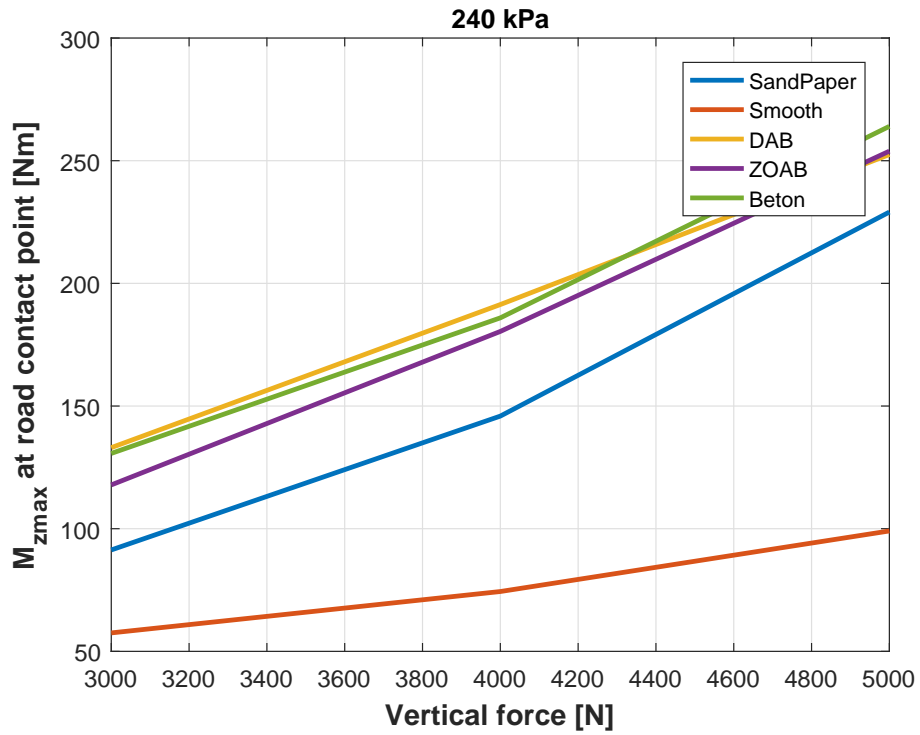
Figure 5.1: Tyre 1: $M_{z,peak}$ vs F_z at inflation pressure of 240 kPa
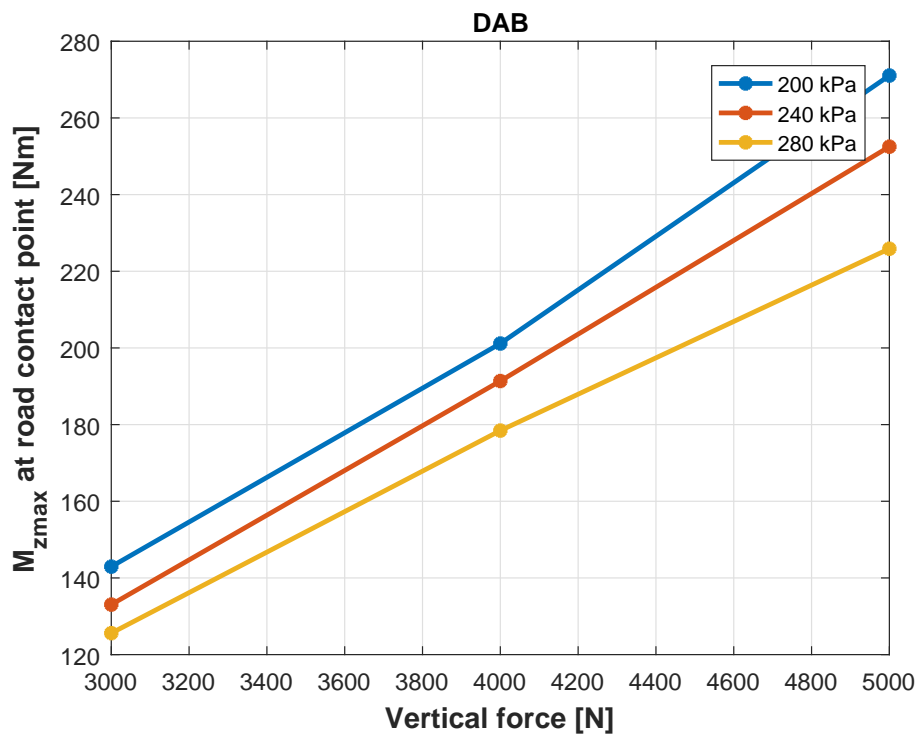
Figure 5.2: Tyre 1: $M_{z,peak}$ vs F_z DAB surface
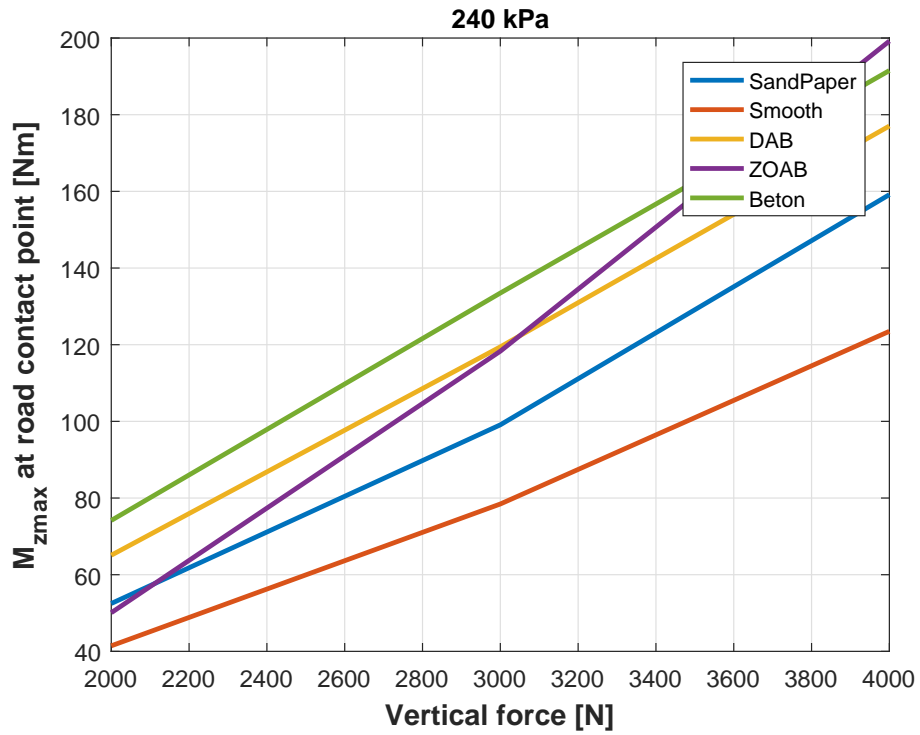
Figure 5.3: Tyre 2: $M_{z,peak}$ vs F_z at inflation pressure of 240 kPa
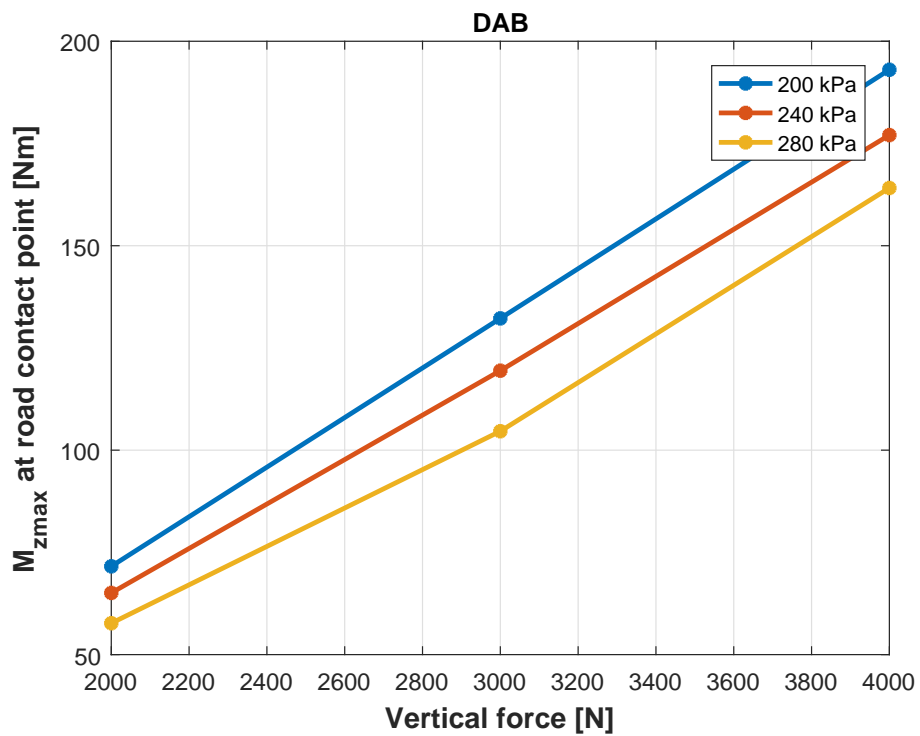
Figure 5.4: Tyre 2: $M_{z,peak}$ vs F_z DAB surface
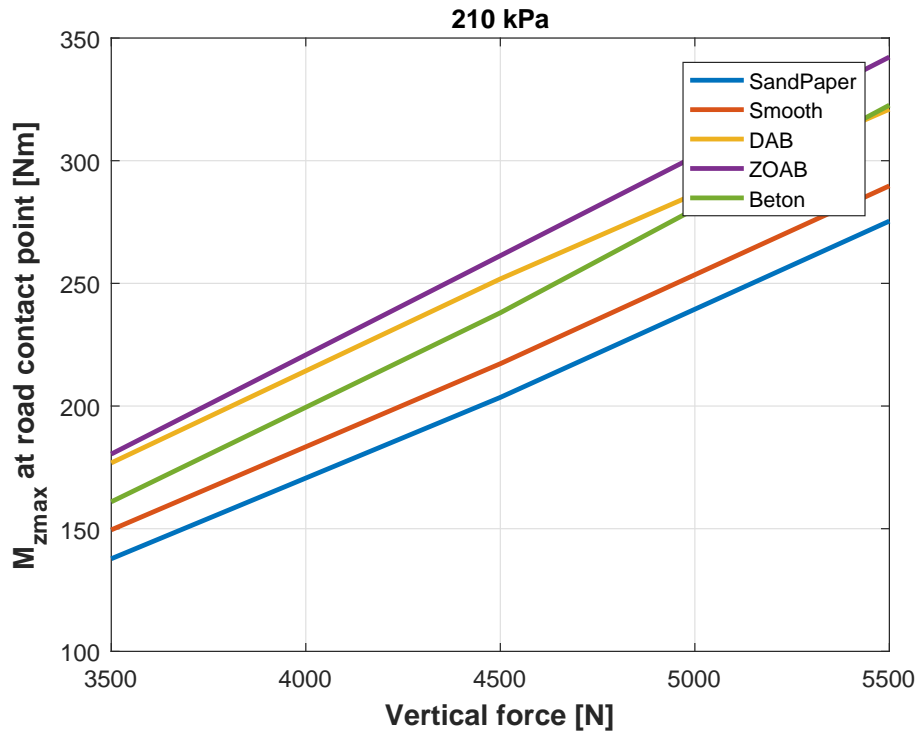
Figure 5.5: Tyre 3: $M_{z,peak}$ vs F_z at inflation pressure of 210 kPa
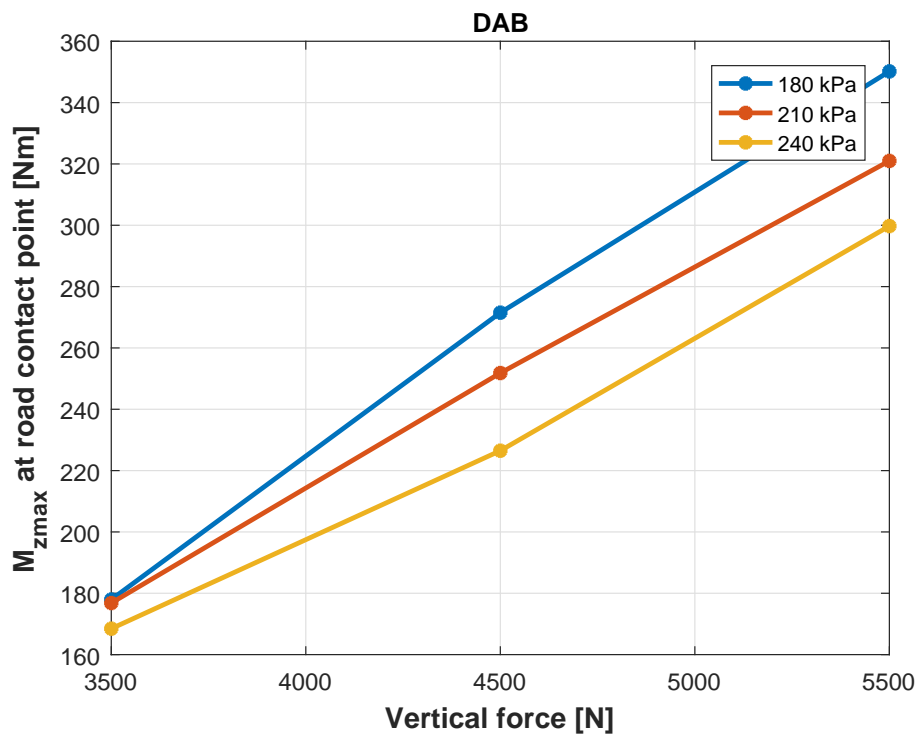
Figure 5.6: Tyre 3: $M_{z,peak}$ vs F_z DAB surface

5.3   Aligning stiffness

The aligning stiffness $(C_{M\alpha})$ can be calculated using:

$$M_z = -C_{M\alpha}\alpha \tag{5.1}$$

Here, since it is standstill conditions, we replace the slip angle (α) with the yaw angle (ψ):

$$C_{M\alpha} = -\frac{M_z}{\psi} \tag{5.2}$$

Using equation (5.2), the the aligning stiffness as a function of inflation pressure and vertical force was plotted in figures 5.7 (Tyre 1), 5.8 (Tyre 2) and 5.9 (Tyre 3). It is observed that $C_{M\alpha}$ increases with increase in the applied vertical force. However, the aligning stiffness reduces as the inflation pressure increases.
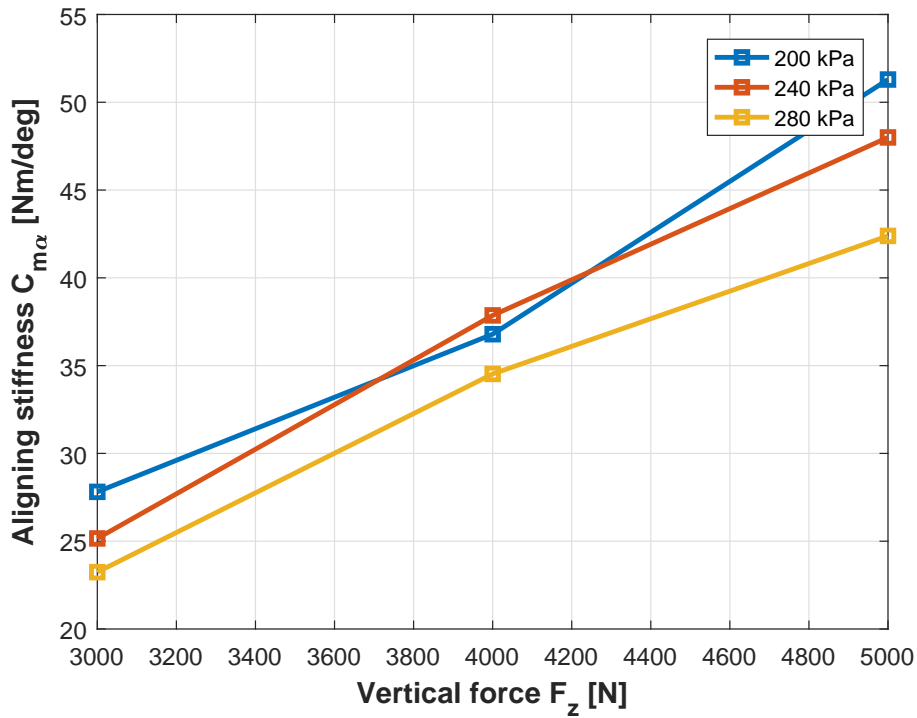
Figure 5.7: Tyre 1: $C_{M\alpha}$ vs vertical force F_z
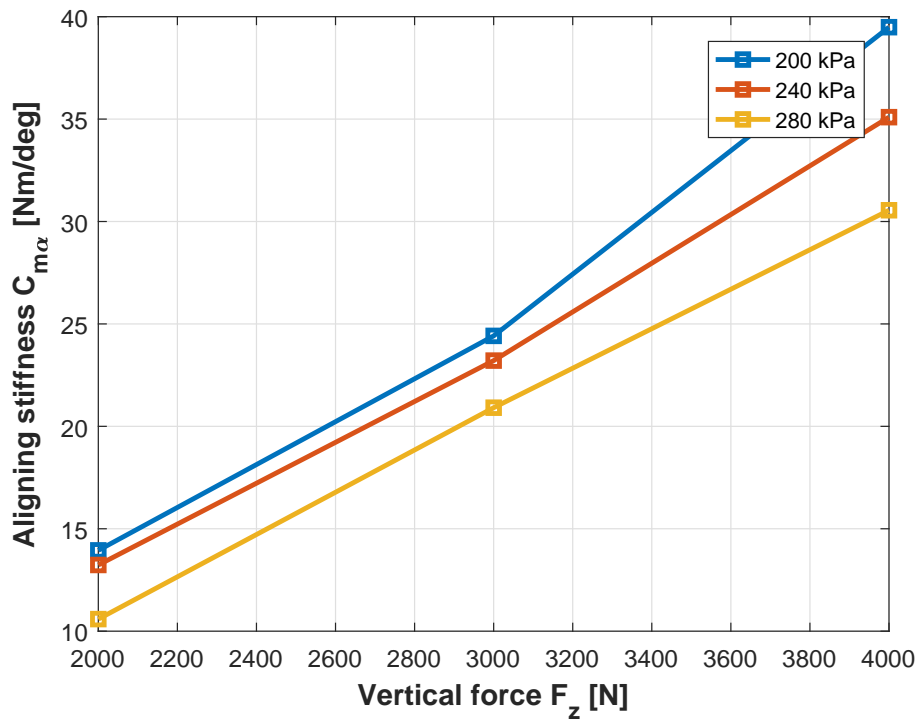
Figure 5.8: Tyre 2: $C_{M\alpha}$ vs vertical force F_z
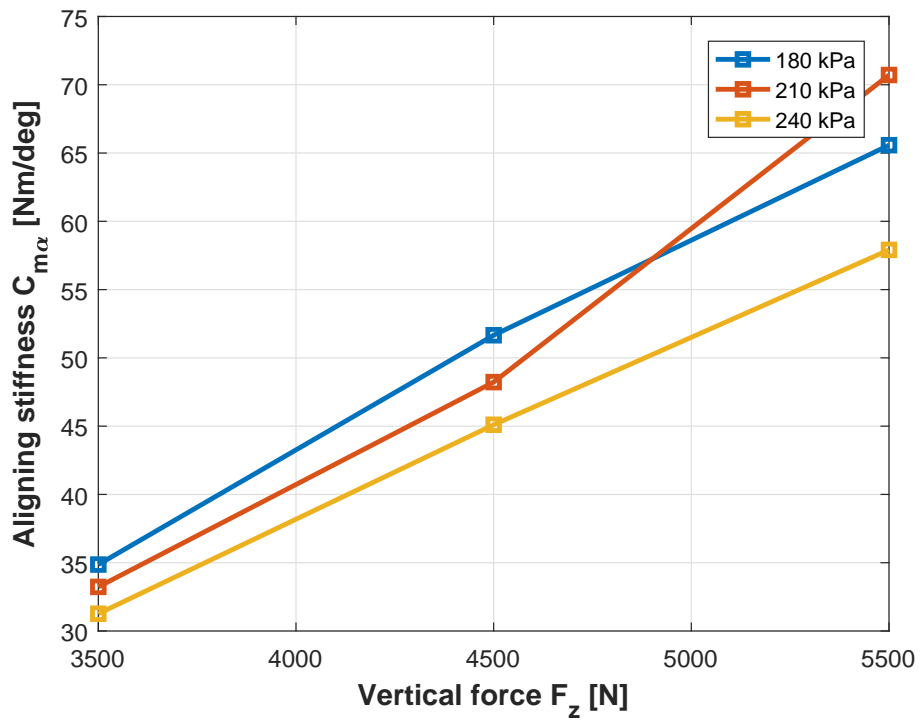
Figure 5.9: Tyre 3: $C_{M\alpha}$ vs vertical force F_z

Influence of different road surface types on tyre turn slip & friction characteristics   19

5.4   Contact patch dimensions

To calculate the peak friction coefficient in section 5.5, the contact patch dimensions of the tyres need to be known.

The contact patch dimension is dependent on the applied vertical force and inflation pressure of the tyre. The tyre property files for Tyre 1 and Tyre 2 were available from TASS International and the equations for calculating the contact patch dimensions were made available. However, the pressure dependency parameter was 0 in the tyre property files. So, according to the tyre property files, the contact patch of Tyre 1 and Tyre 2 only depends on the applied vertical force and does not change with a variation in inflation pressure.

The contact patch dimensions of Tyre 3 was found by painting the tyre and applying vertical force for different inflation pressures on a white paper. Figure 5.10 shows the contact patch print of Tyre 3 at an inflation pressure of 240 kPa and vertical force of 3500 N. The contact patch dimensions of all the tyres at different vertical loads and inflation pressures are listed in table 5.1 where a is half of contact patch length and b is half of contact patch width. It can be observed in table 5.1, the contact patch of Tyre 3, which was measured shows variation due to inflation pressure change.

Figure 5.10: Tyre 3 contact patch at Inflation pressure: 240 kPa and Vertical force: 3500 N

Table 5.1: Contact patch dimensions

Tyre 1	3000 N	4000 N	5000 N
200 kPa	a = 0.0571 m b = 0.0594 m	a = 0.0661 m b = 0.0616 m	a = 0.0742 m b = 0.0626 m
240 kPa	a = 0.0571 m b = 0.0594 m	a = 0.0661 m b = 0.0616 m	a = 0.0742 m b = 0.0626 m
280 kPa	a = 0.0571 m b = 0.0594 m	a = 0.0661 m b = 0.0616 m	a = 0.0742 m b = 0.0626 m
Tyre 2	2000 N	3000 N	4000 N
200 kPa	a = 0.0428 m b = 0.0567 m	a = 0.0533 m b = 0.0629 m	a = 0.0623 m b = 0.0674 m
240 kPa	a = 0.0428 m b = 0.0567 m	a = 0.0533 m b = 0.0629 m	a = 0.0623 m b = 0.0674 m
280 kPa	a = 0.0428 m b = 0.0567 m	a = 0.0533 m b = 0.0629 m	a = 0.0623 m b = 0.0674 m
Tyre 3	3500 N	4500 N	5500 N
180 kPa	a = 0.0715 m b = 0.0785 m	a = 0.0855 m b = 0.0800 m	a = 0.0960 m b = 0.0820 m
210 kPa	a = 0.0675 m b = 0.0775 m	a = 0.0785 m b = 0.0795 m	a = 0.0825 m b = 0.0810 m
240 kPa	a = 0.0650 m b = 0.0750 m	a = 0.0750 m b = 0.0790 m	a = 0.0800 m b = 0.0800 m

5.5 Peak friction estimation

To observe the differences caused by a variation of the road surface and be able to identify parameters for turn slip model, the peak frictions were identified. The friction coefficient (μ) was calculated using equation (5.10). In equation (5.10), the following assumptions were made:

1. Uniform vertical load and pressure throughout the contact patch.

2. Uniform coefficient of friction thoughout the contact patch.

3. The contact patch ellipse is assumed to be circular of same surface area.

For the estimation of the contact patch:
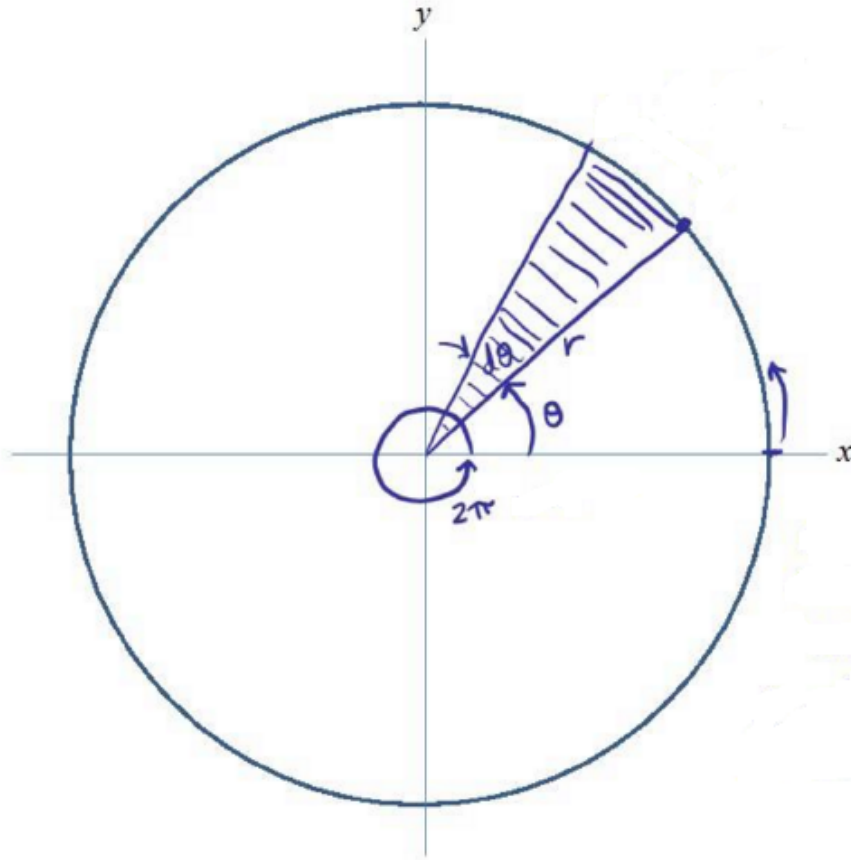
Figure 5.11: Circular contact patch

We get:

$$M_z = \int_0^r \int_0^{2\pi} \mu.\rho.P.d\rho.\rho.d\theta \tag{5.3}$$

Where, ρ is the distance of the point from the centre of the contact patch, ranging from 0 to r, where, r is the radius of the contact patch circle. P is the pressure. Using the assumptions and $P = F_z/A$, where F_z is the vertical load and A is the area.

$$M_z = \mu\frac{Fz}{A}\int_0^r \int_0^{2\pi} \rho^2.d\rho.d\theta \tag{5.4}$$

Gives:

$$M_z = \frac{2}{3}\mu.F_z.r \tag{5.5}$$

Hence,

$$\mu = \frac{3}{2}\frac{M_z}{F_z r} \tag{5.6}$$

In this calculation, the contact patch is assumed to be circular. It is converted to an elliptical patch with the same surface area of the assumed circular patch.

$$A_{ellipse} = A_{circle} \tag{5.7}$$

Where, A is the contact patch area.

$$\pi.a.b = \pi.r^2 \tag{5.8}$$

$$M_z = \frac{2}{3}\mu F_z \sqrt{a.b} \tag{5.9}$$

Therefore,

$$\mu = \frac{3}{2}\frac{M_z}{F_z\sqrt{a.b}} \tag{5.10}$$

Where, F_z is the applied vertical force, a is the half of contact patch length and b is the half of contact patch width.

However, it must be noted that this approximation is not accurate and some error is present as can be seen in table 5.1. The friction coefficients are calculated and plotted for different surfaces and operating conditions:
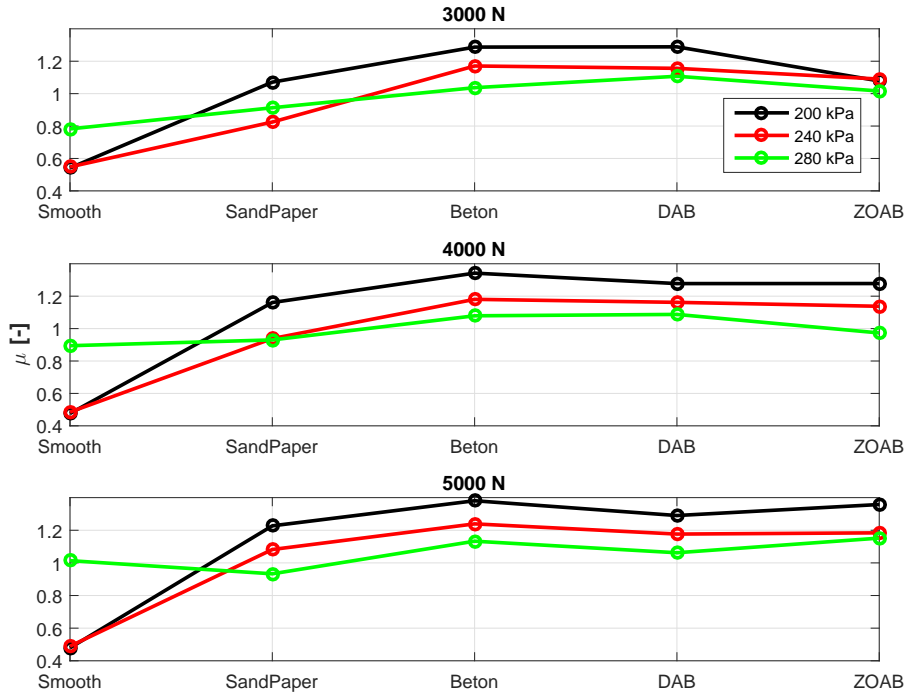
Figure 5.12: Tyre 1 friction coefficient comparison for different inflation pressures and road surfaces
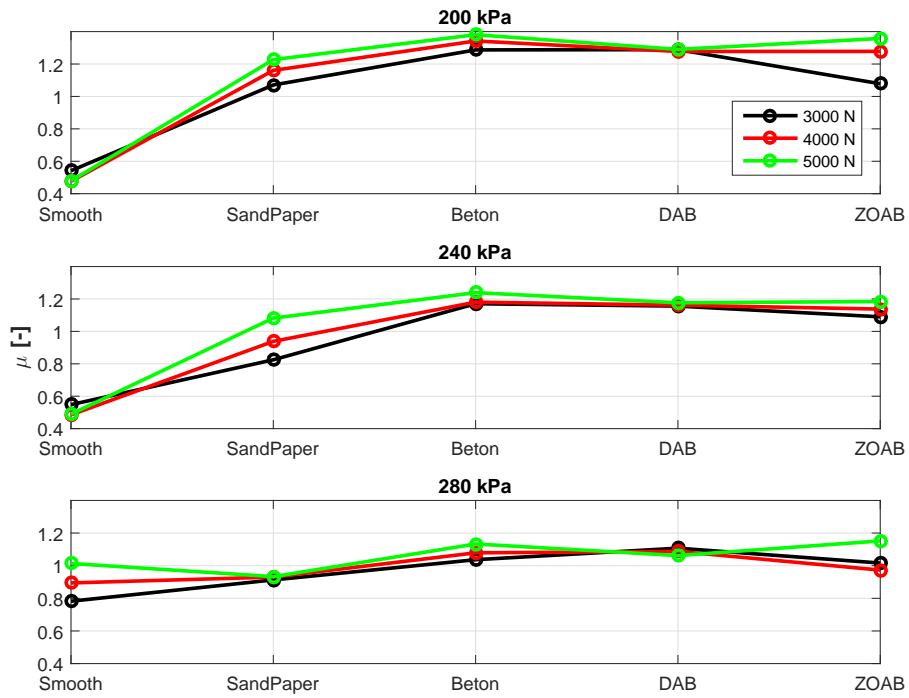
Figure 5.13: Tyre 1 friction coefficient comparison for different vertical forces and road surfaces
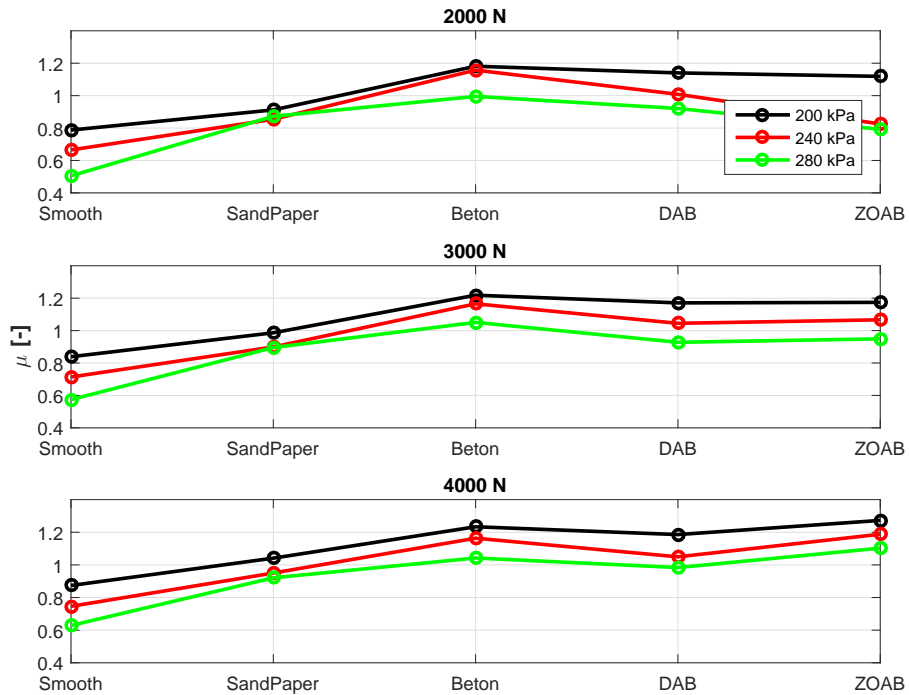
Figure 5.14: Tyre 2 friction coefficient comparison for different inflation pressures and road surfaces
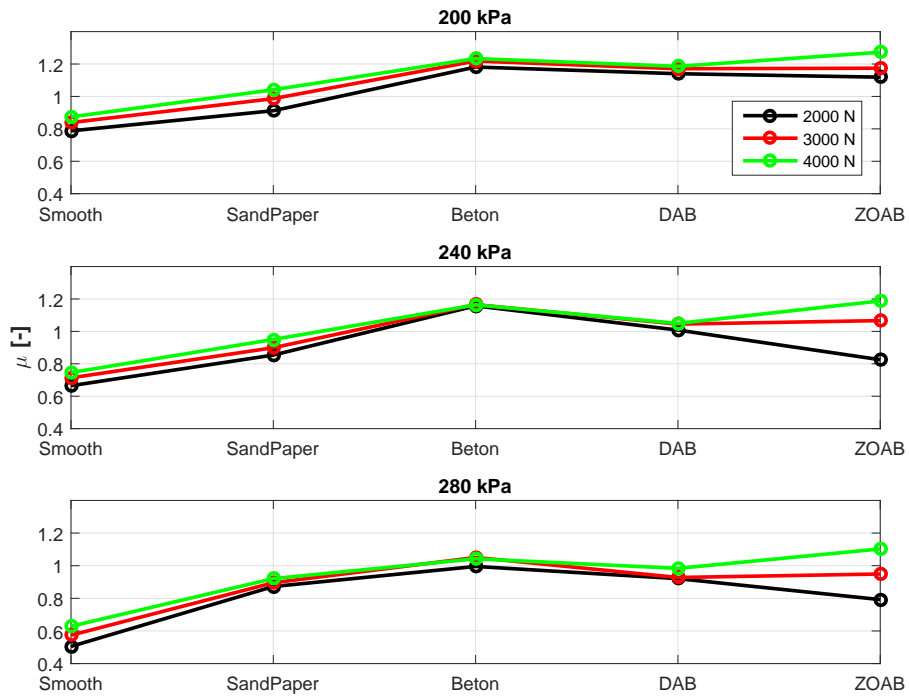
Figure 5.15: Tyre 2 friction coefficient comparison for different vertical forces and road surfaces
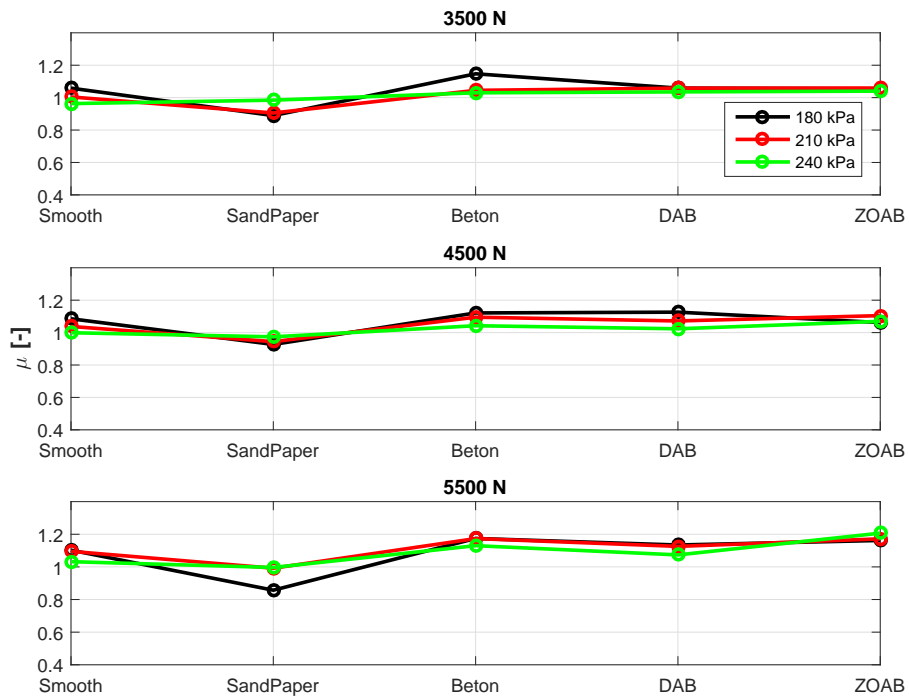
Figure 5.16: Tyre 3 friction coefficient comparison for different inflation pressures and road surfaces
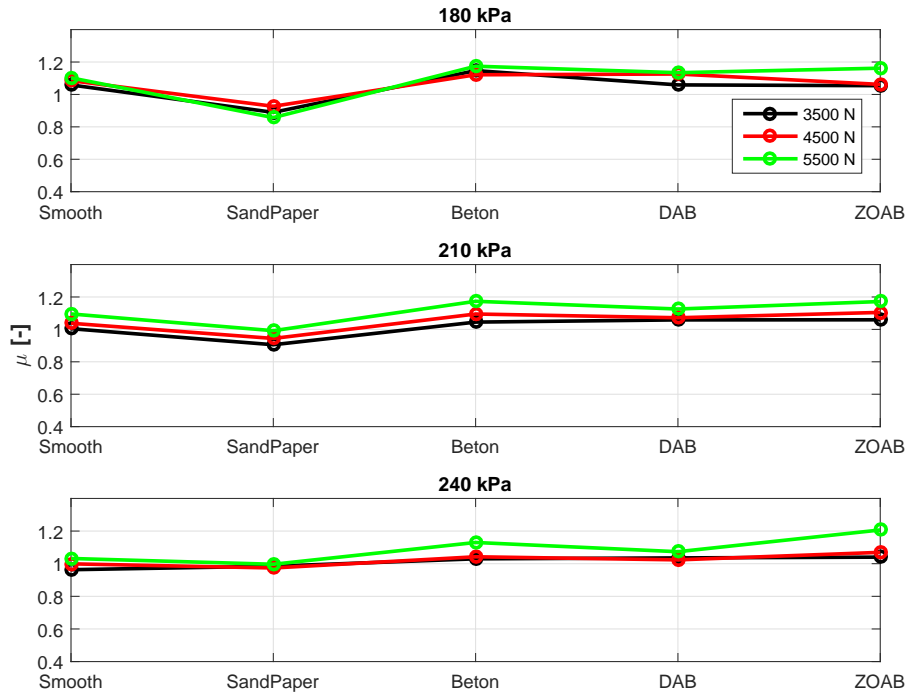
Figure 5.17: Tyre 3 friction coefficient comparison for different vertical forces and road surfaces

It can be observed from figures 5.11 to 5.16 that as the vertical force increases, the peak friction coefficient increases. This is in accordance with Persson's hysteresis theory [7], as described in section 2.3. When the inflation pressure increases, the friction coefficient decreases. This is because of the non-uniform distribution of pressure across the contact patch as the inflation pressure increases. There is a larger contact pressure at the centre which decreases towards the edge of the contact patch.

The peak friction values between the tyres are compared for their nominal force and inflation pressure.This comparison is shown in figure 5.17: Since, the ZOAB surface was damaged, it was decided to compare the results from the SandPaper, Beton and DAB surfaces. It can be seen that for all tyres, the friction coefficient with the Beton surface is higher or at times comparable with the DAB surface. It can also be observed that the Beton surface shows a higher friction coefficient than the SandPaper. However, the difference in friction on different surfaces is strongly dependent on the tyre and it's operating conditions.

To scale the friction coefficient between different road surfaces, the peak friction coefficient vs the local contact pressure was plotted for each tyre. This was done for the SandPaper, DAB and Beton surfaces. Assuming an uniform pressure distribution through the contact patch and an elliptical contact patch shape, the local contact pressure was calculated by dividing F_z by the contact patch area. The resulting plots can be seen in figures 5.18, 5.19 & 5.20. The local contact pressure (P_{local}) was calculated as:

$$P_{local} = \frac{F_z}{\pi.a.b} \tag{5.11}$$
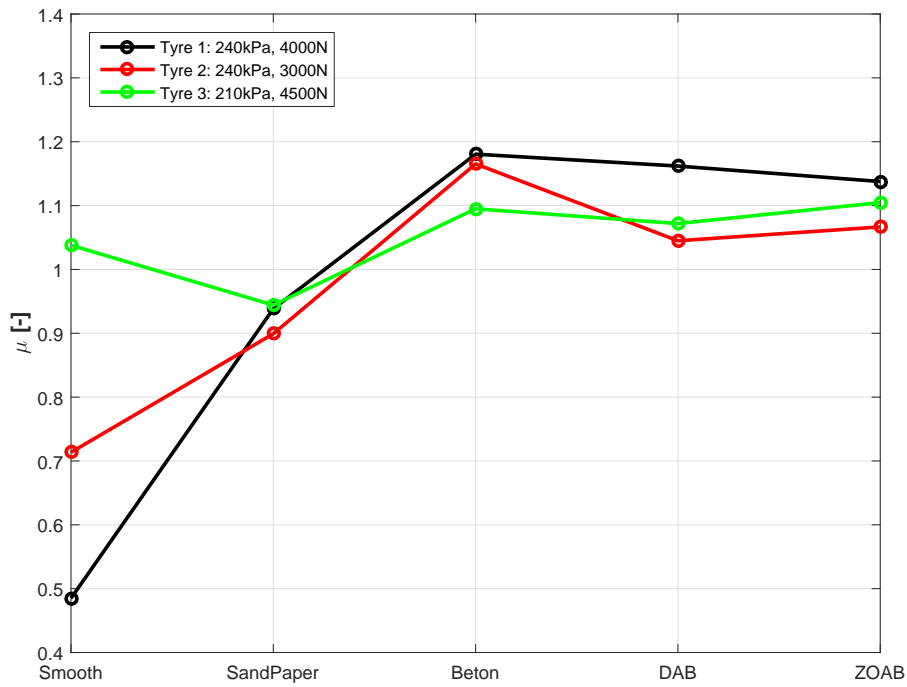
Figure 5.18: Peak friction coefficients at their nominal loads
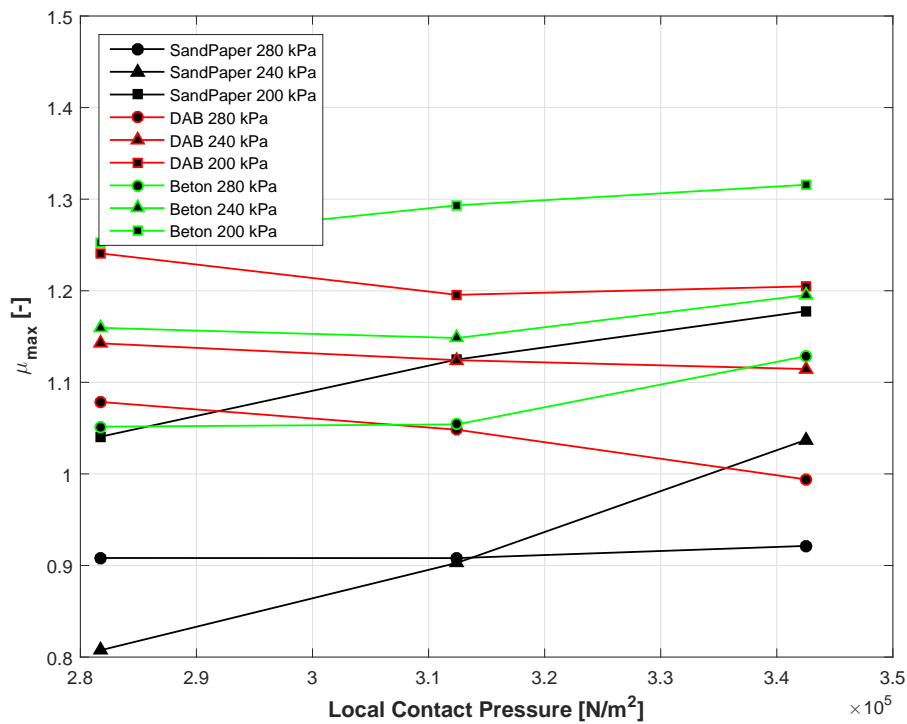
Figure 5.19: Tyre 1: Friction coefficient μ vs Local contact pressure
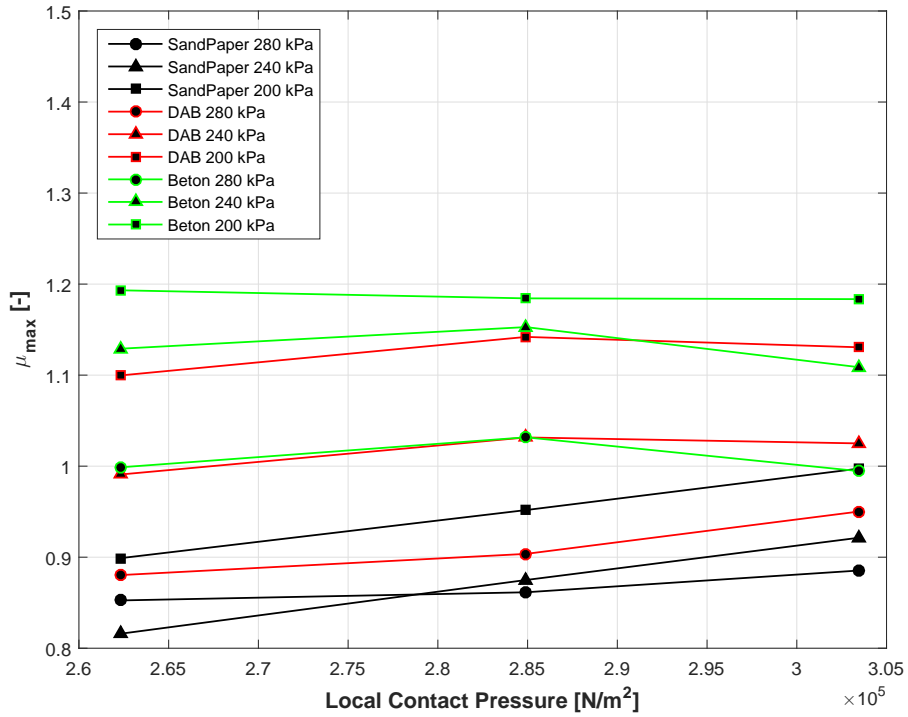
Figure 5.20: Tyre 2: Friction coefficient μ vs Local contact pressure
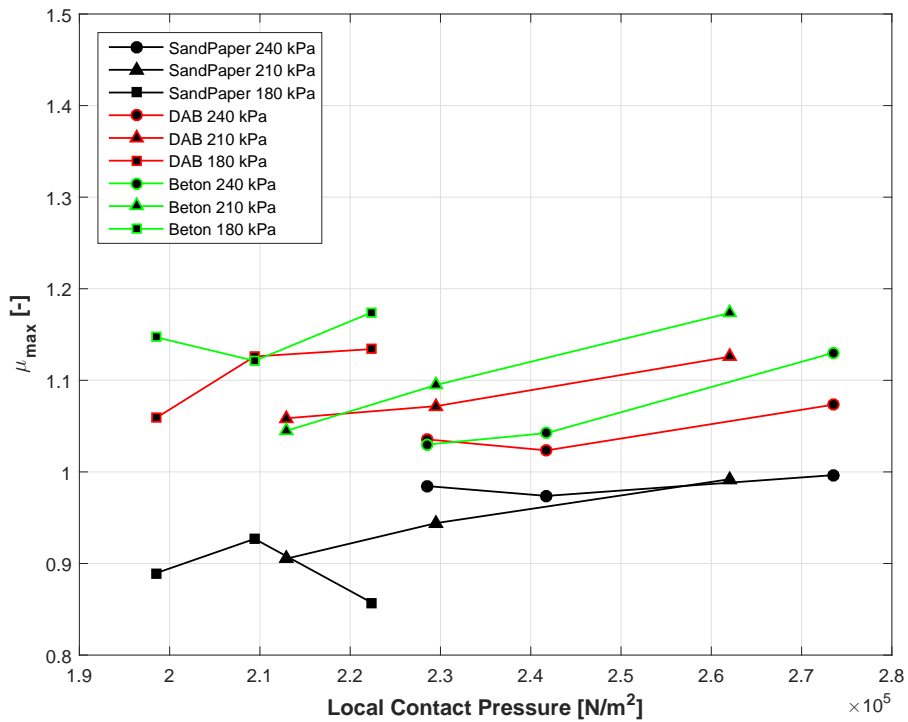
Figure 5.21: Tyre 3: Friction coefficient μ vs Local contact pressure

In figure 5.18 and 5.19, it can be seen that for the same local contact pressure (applied vertical load divided by the contact patch area), three different friction coefficients are observed for each surface. This is because Tyre 1 and Tyre 2 property files do not model the effect of inflation pressure change on the contact patch. This is not observed in Tyre 3, whose contact patch was measured.

It is important to have the inflation pressure dependency on the contact patch. The scaling of the friction is highly dependent on the tyre properties.

Chapter 6

Conclusions and recommendations

6.1   Conclusions

The road surface's friction influences the moment generated by the tyre during a parking manoeuvre. It is observed that the Beton surface generally has a higher friction coefficient than the DAB surface. Since the ZOAB surface was damaged during the measurements, it has not been used when comparing friction coefficients. However, the measurement data is made available for the ZOAB surface to the reader for their reference.

It is observed that the frictional forces generated by the tyre are dependent on the contact mechanics, which are dependent on the following:

1. Vertical force.

2. Actual contact area.

3. Tyre properties

The following conclusions are drawn for the turn slip measurements at standstill conditions:

1. The Beton surface has a higher friction coefficient than the DAB surface.

2. Beton has a higher friction coefficient than SandPaper.

3. The friction coefficient (μ) increases as the applied vertical load increases.

4. The dependency of friction between different surfaces is strongly dependent on the tyre and it's operating conditions.

6.2   Recommendations

Each surface has a single sample available for measurements. After each measurement, the rubber would get laid onto the surface. This may affect the results, since the "rubbering" of the road surface would change the frictional force generation.

To have a better understanding of the effect of the surface roughness, it is recommended to do the measurements on the following surface conditions:

1. New surface: when the surface is freshly laid.

2. Used surface: after some rubber has been laid on the surface after extensive use.

3. Dirty surface: the presence of dirt on the surface could affect the frictional force generation.

4. Wet surface: the presence of a water film between the surface and tyre could affect the frictional force generation.

It is also recommended to get the road surface scanned for it's roughness measurement. Having the surface power spectrum would help in understanding the difference in frictional force generation on different surfaces. For future work, it is advised to have a better estimation of the contact patch area. Lastly, it would be interesting to observe the effect of change in the sliding velocity.

Bibliography

[1] P. van der Jagt. The Road to Virtual Vehicle Prototyping, Ph.D thesis, Mechanical Engineering Department, Eindhoven University of Technology, 2000.

[2] H.W. Kummer. *Unified Theory of Rubber and Tire Friction*. Number no. 94 in Engineering research bulletin. Pennsylvania State University, College of Engineering, 1966.

[3] B. Lorenz, Y. R. Oh, S. K. Nam, S. H. Jeon, and B. N. J. Persson. Rubber friction on road surfaces: Experiment and theory for low sliding speeds. *The Journal of Chemical Physics*, 142(19), 2015.

[4] Carlo Lugaro, Antoine Schmeitz, Toshiya Ogawa, Tetsuya Murakami, and Sonny Huisman. Development of a parameter identification method for mf-tyre/mf-swift applied to parking and low speed manoeuvres. *SAE Int. J. Passeng. Cars - Mech. Syst.*, 9:892–902, 04 2016.

[5] D. F. Moore. The friction and lubrication of elastomers. pergamon, oxford. 1972. 288 pp. illustrated. £7.50. *The Aeronautical Journal (1968)*, 79(769):45, 001 1975.

[6] Hans B. Pacejka. *Tire and Vehicle Dynamics (Third Edition)*. Butterworth-Heinemann, Oxford, 2012.

[7] B. N. J. Persson. Theory of rubber friction and contact mechanics. *The Journal of Chemical Physics*, 115(8), 2001.

[8] A.J.C. Schmeitz, I.J.M. Besselink, J. de Hoogh, and H. Nijmeijer. Extending the Magic Formula and Swift tyre models for inflation pressure changes. 2005.

[9] R. S. Sharp, P. Gruber, and E. Fina. Circuit racing, track texture, temperature and rubber friction. *Vehicle System Dynamics*, 54(4):510–525, 2016.

[10] TASS International. MF-Tyre/MF-Swift (Version 6.2). https://www.tassinternational.com/delft-tyre.

Appendix A

Measurement results

The self aligning moment (M_z) vs yaw angle plots for the tyres are shown here:
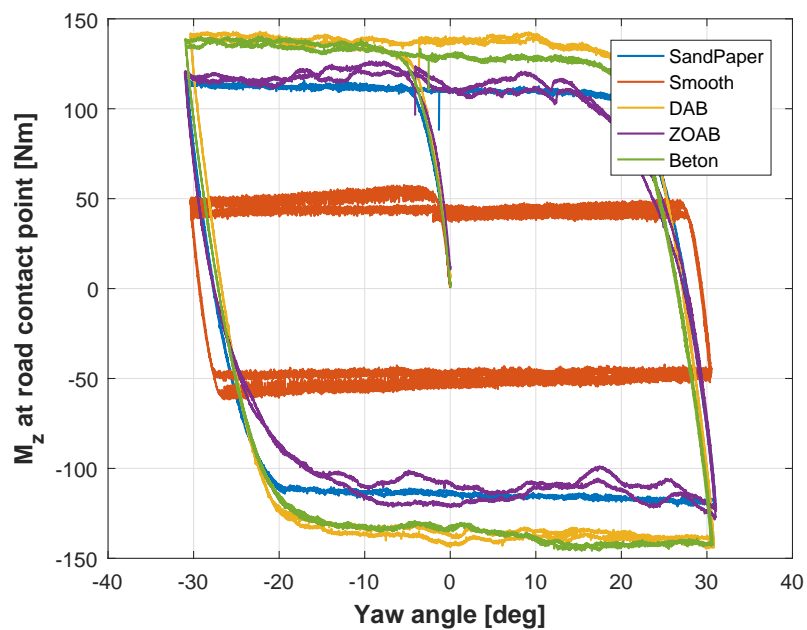
Figure A.1: Tyre 1 M_z vs ψ (Inflation pressure: 200 kPa, Vertical force: 3000 N)
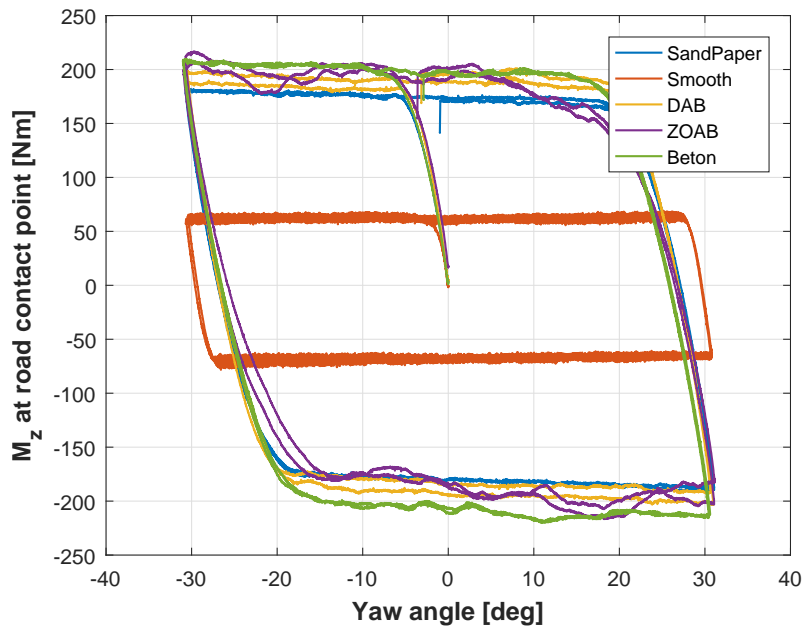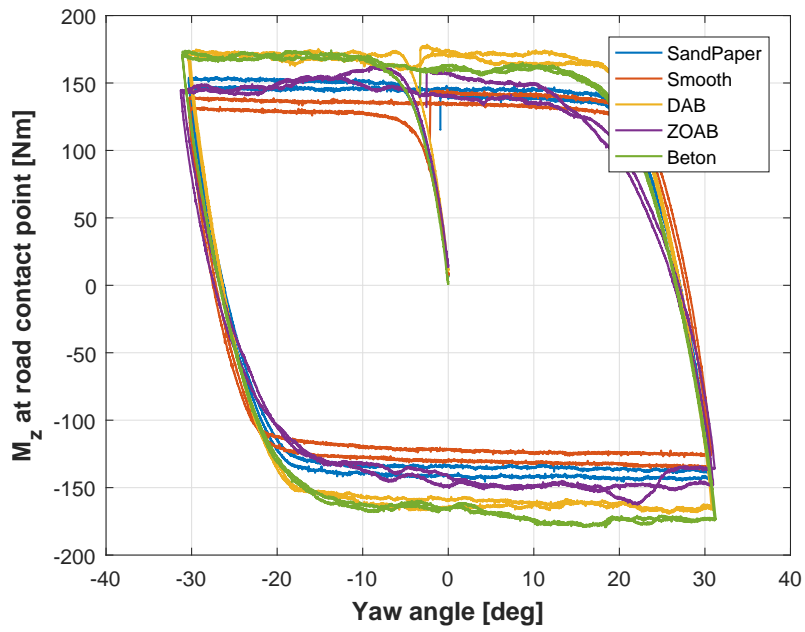
Figure A.2: Tyre 1 M_z vs ψ (Inflation pressure: 200 kPa, Vertical force: 4000 N)
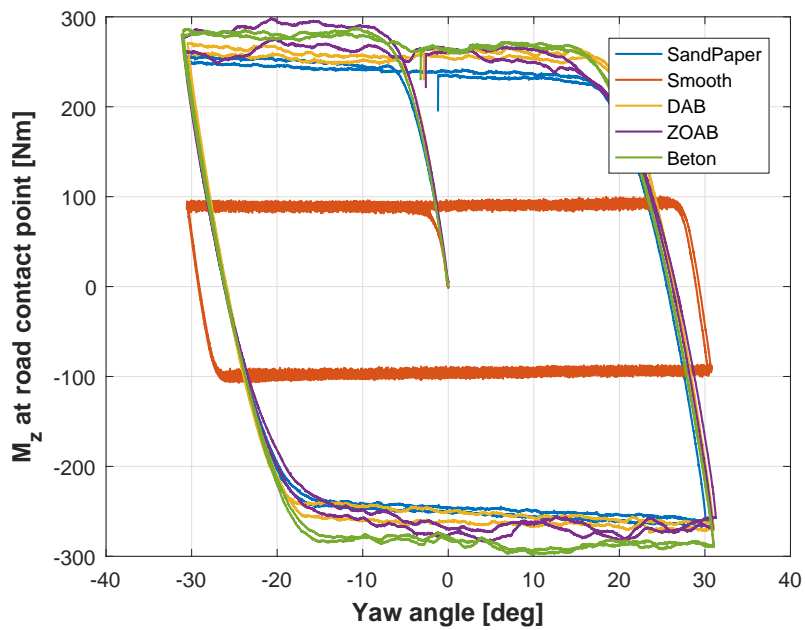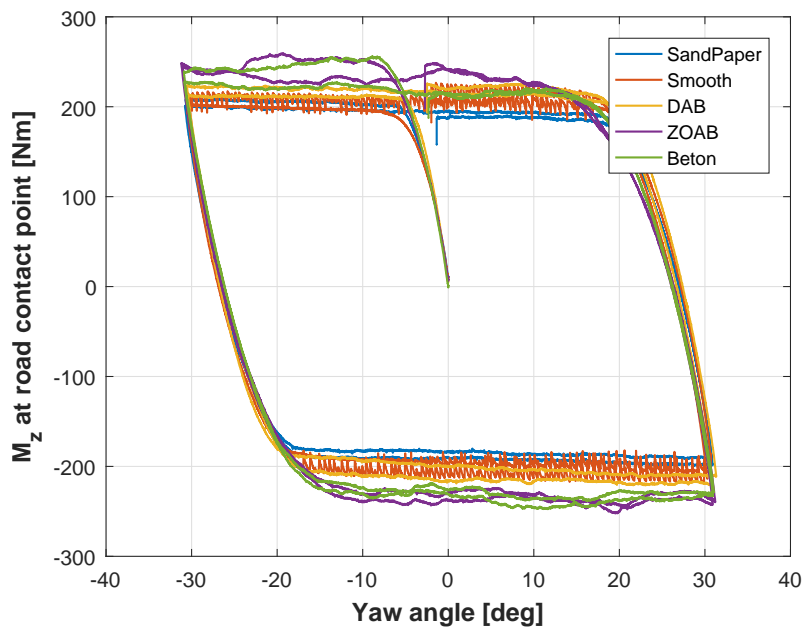

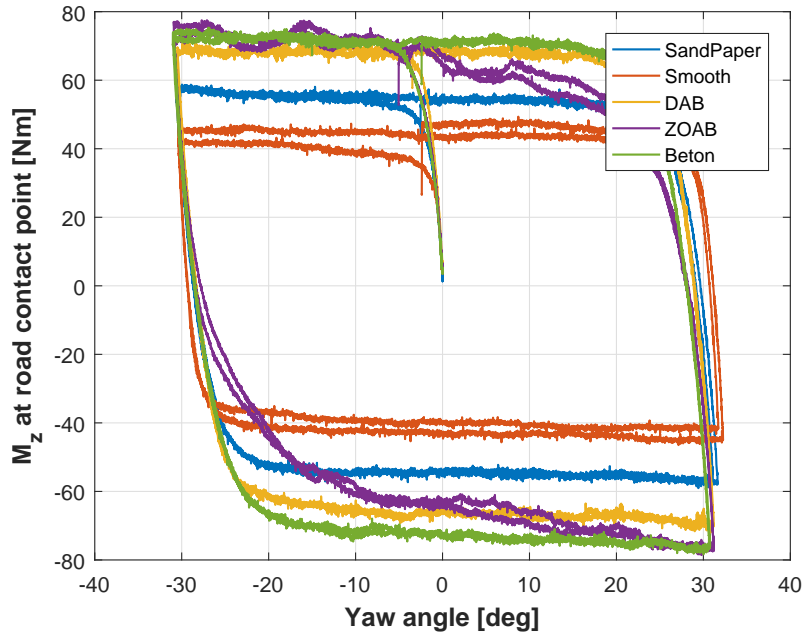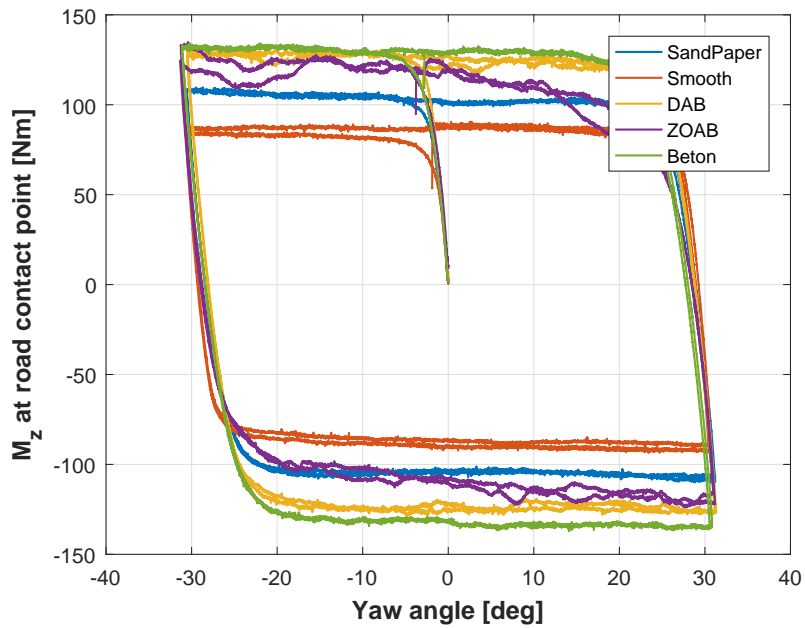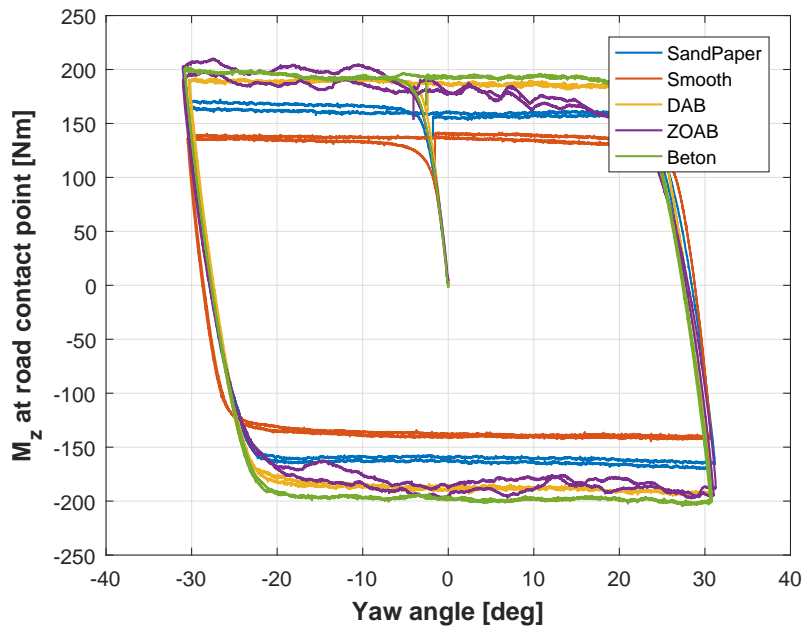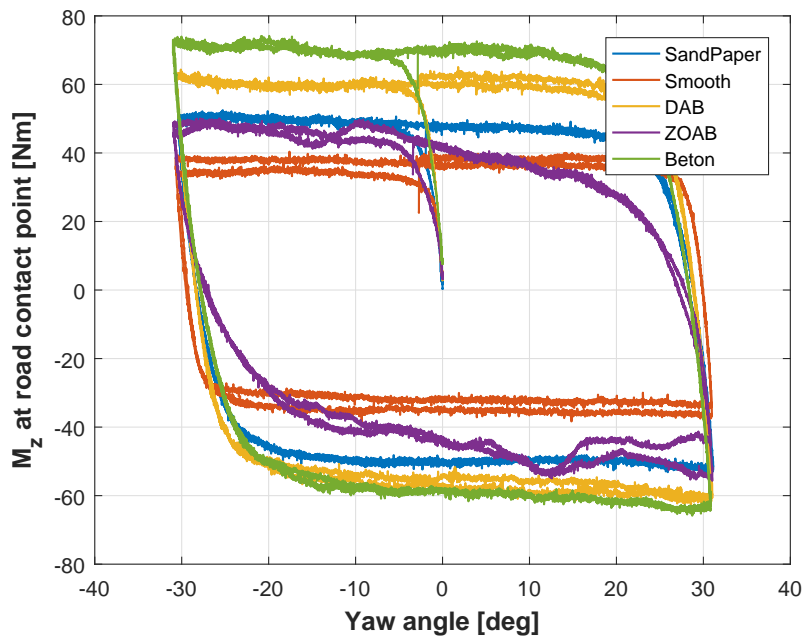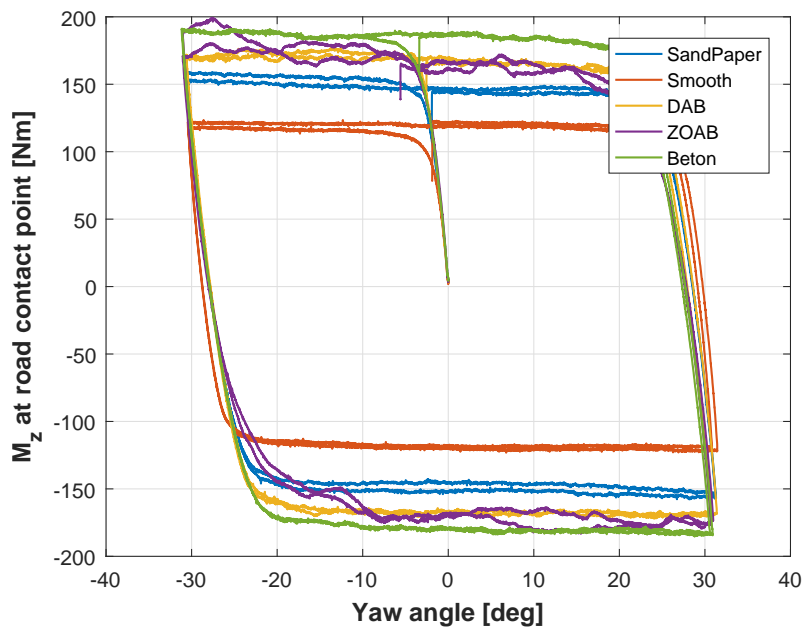Figure A.3: Tyre 1 M_z vs ψ (Inflation pressure: 200 kPa, Vertical force: 5000 N)
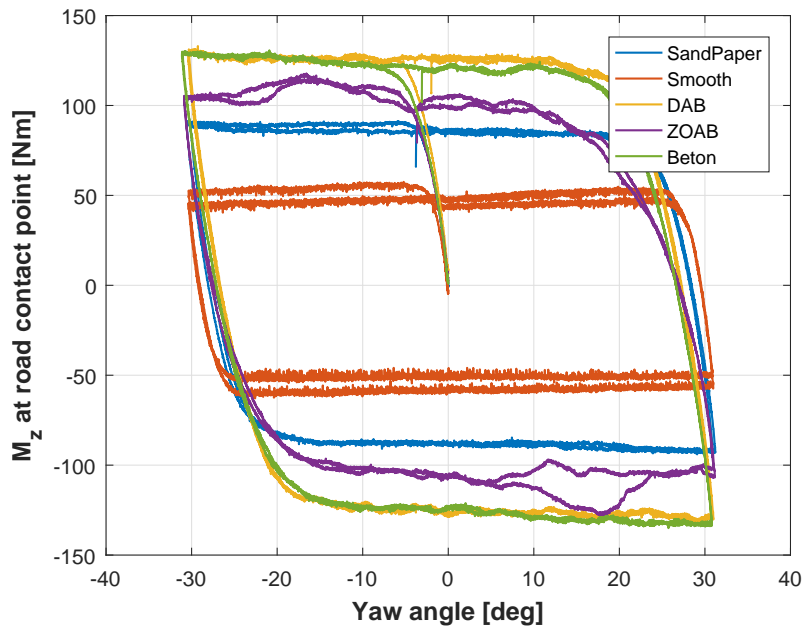
Figure A.4: Tyre 1 M_z vs ψ (Inflation pressure: 240 kPa, Vertical force: 3000 N)
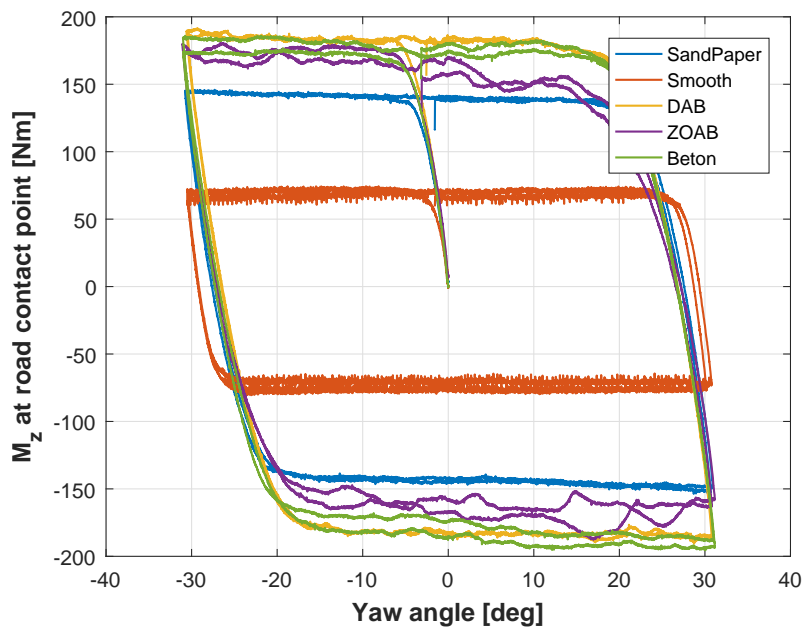
Figure A.5: Tyre 1 M_z vs ψ (Inflation pressure: 240 kPa, Vertical force: 4000 N)
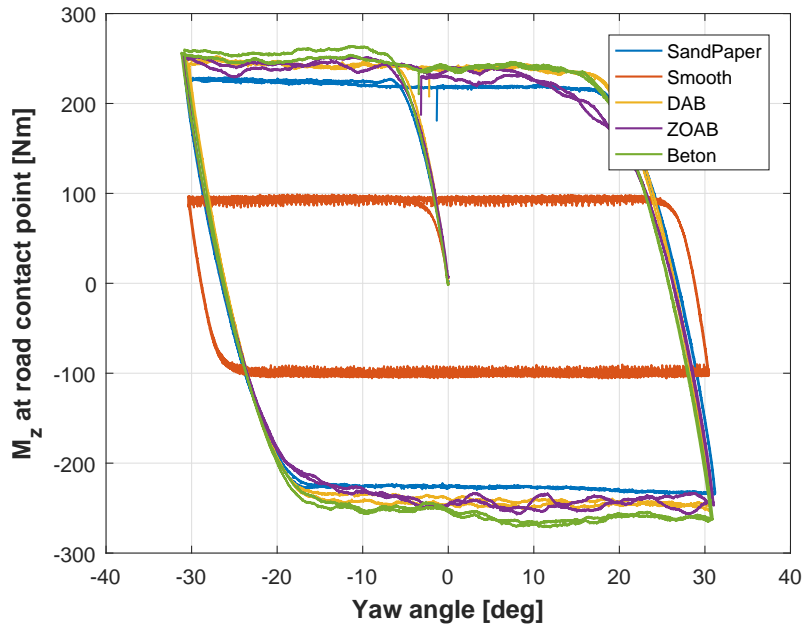
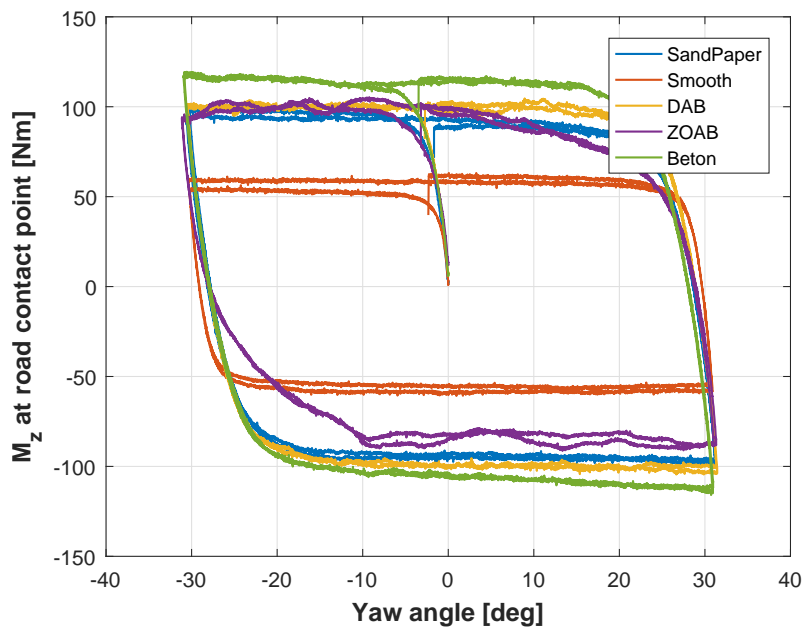Figure A.6: Tyre 1 M_z vs ψ (Inflation pressure: 240 kPa, Vertical force: 5000 N)
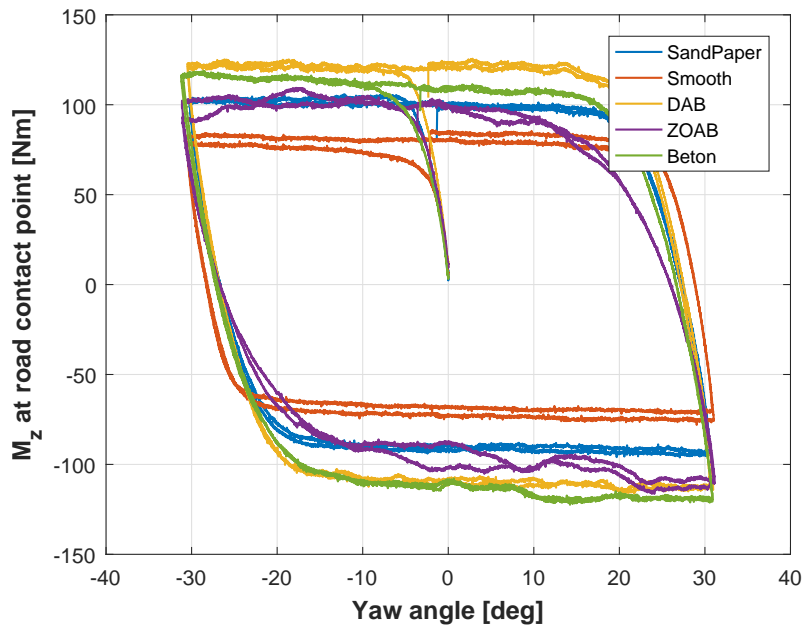
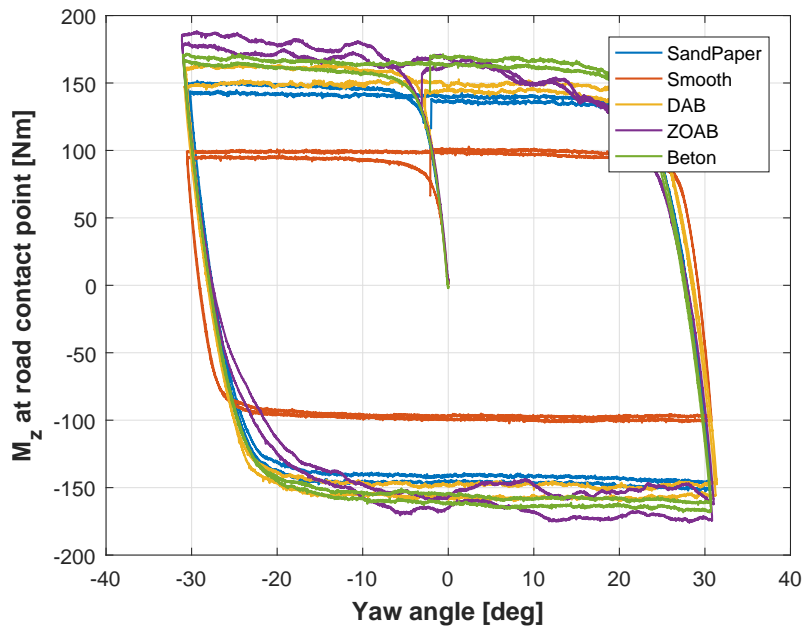Figure A.7: Tyre 1 M_z vs ψ (Inflation pressure: 280 kPa, Vertical force: 3000 N)

Figure A.8: Tyre 1 M_z vs ψ (Inflation pressure: 280 kPa, Vertical force: 4000 N)

Figure A.9: Tyre 1 M_z vs ψ (Inflation pressure: 280 kPa, Vertical force: 5000 N)

Figure A.10: Tyre 2 M_z vs ψ (Inflation pressure: 200 kPa, Vertical force: 2000 N)

Figure A.11: Tyre 2 M_z vs ψ (Inflation pressure: 200 kPa, Vertical force: 3000 N)

Figure A.12: Tyre 2 M_z vs ψ (Inflation pressure: 200 kPa, Vertical force: 4000 N)

Figure A.13: Tyre 2 M_z vs ψ (Inflation pressure: 240 kPa, Vertical force: 2000 N)
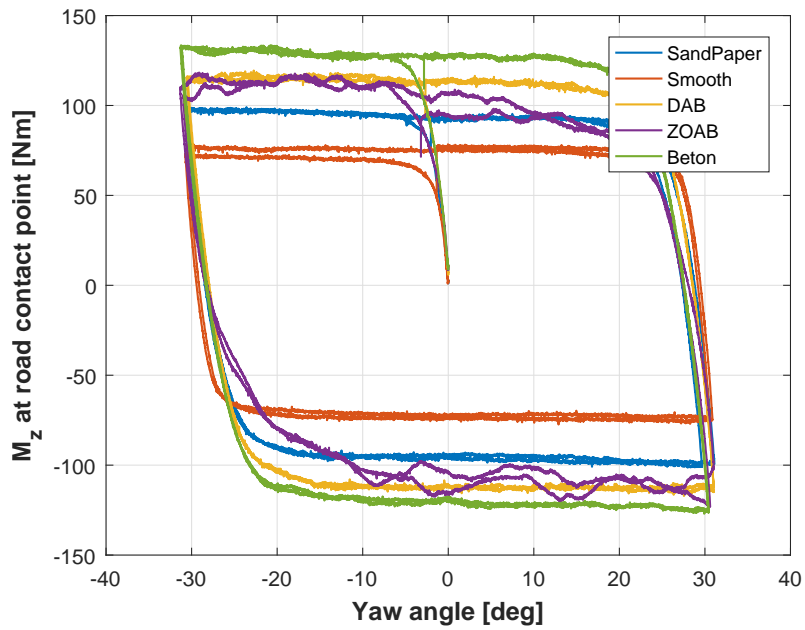
Figure A.14: Tyre 2 M_z vs ψ (Inflation pressure: 240 kPa, Vertical force: 3000 N)

Figure A.15: Tyre 2 M_z vs ψ (Inflation pressure: 240 kPa, Vertical force: 4000 N)
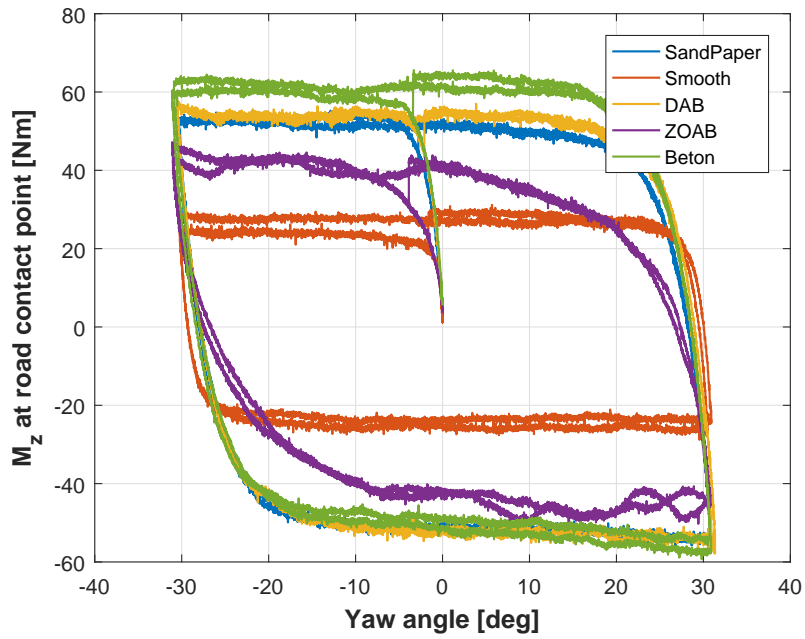
Figure A.16: Tyre 2 M_z vs ψ (Inflation pressure: 280 kPa, Vertical force: 2000 N)
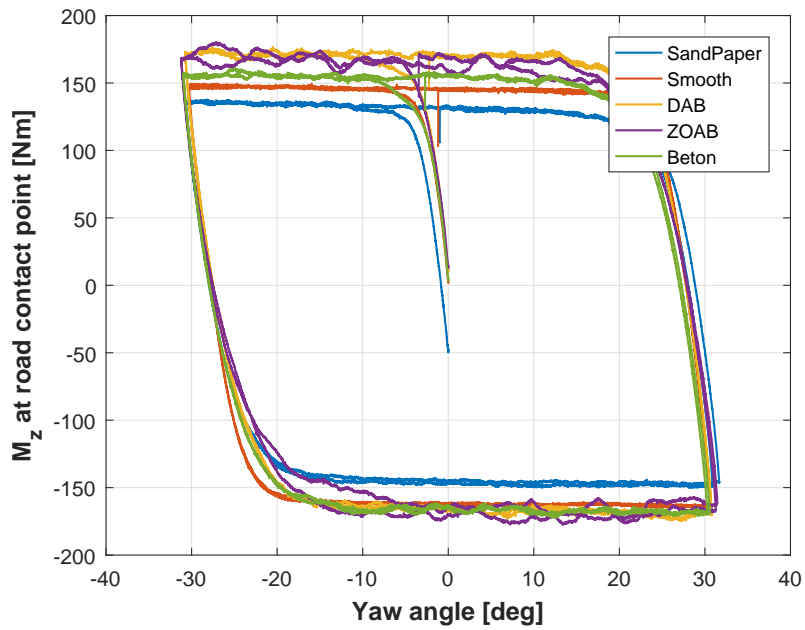

Figure A.17: Tyre 2 M_z vs ψ (Inflation pressure: 280 kPa, Vertical force: 3000 N)

Figure A.18: Tyre 2 M_z vs ψ (Inflation pressure: 280 kPa, Vertical force: 4000 N)
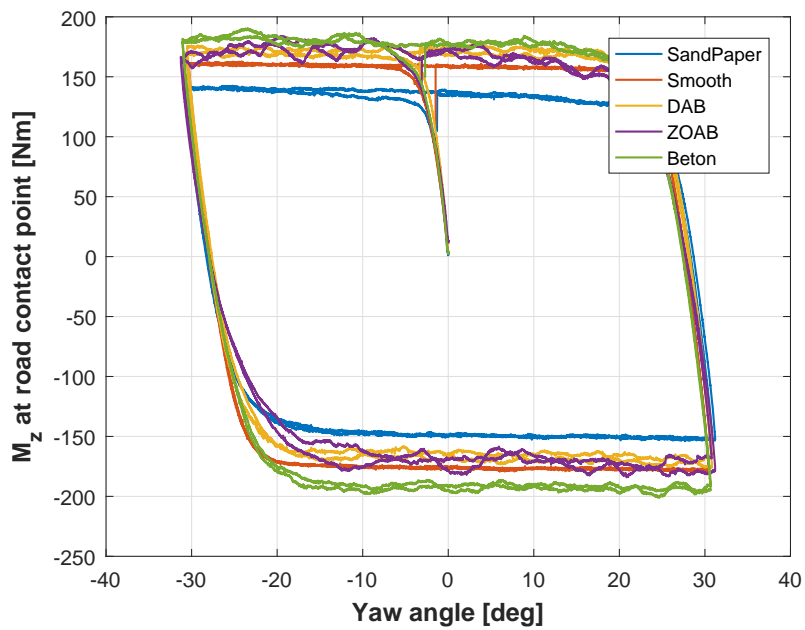
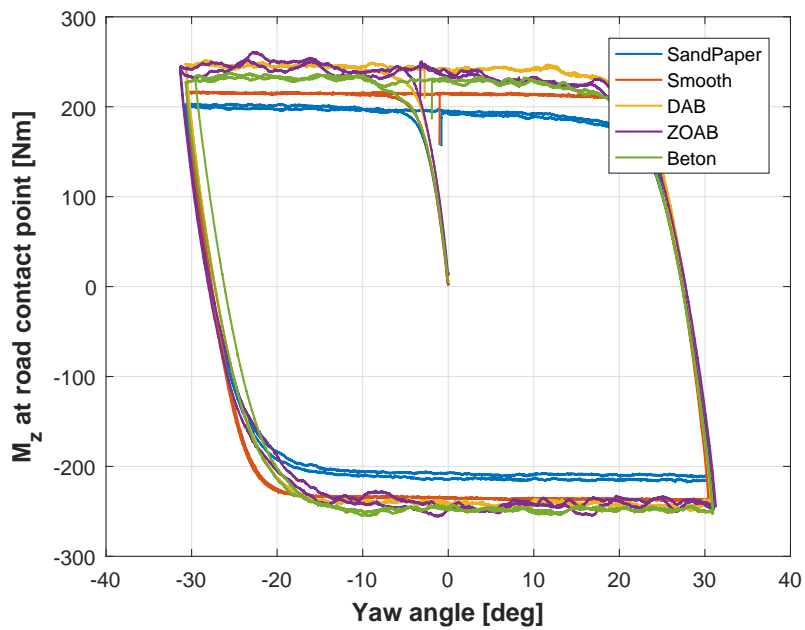Figure A.19: Tyre 3 M_z vs ψ (Inflation pressure: 180 kPa, Vertical force: 3500 N)
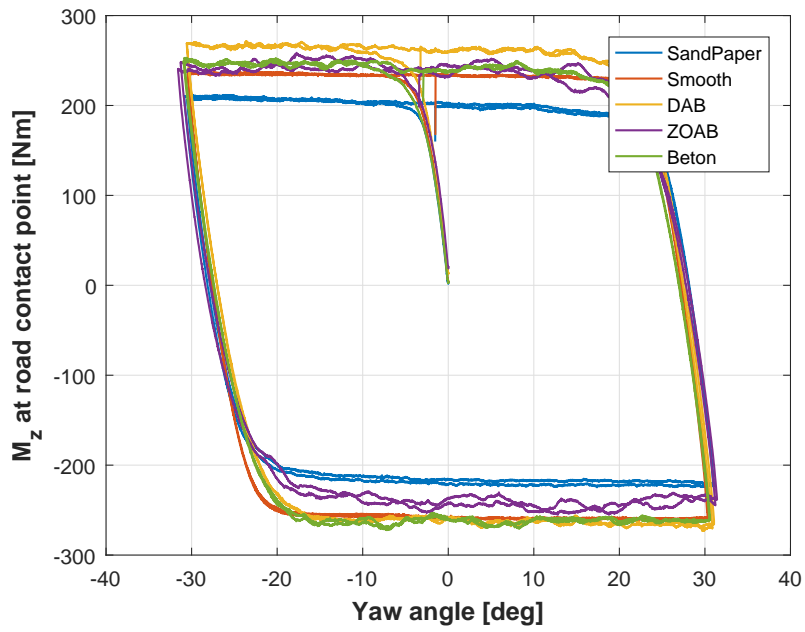
Figure A.20: Tyre 3 M_z vs ψ (Inflation pressure: 180 kPa, Vertical force: 4500 N)
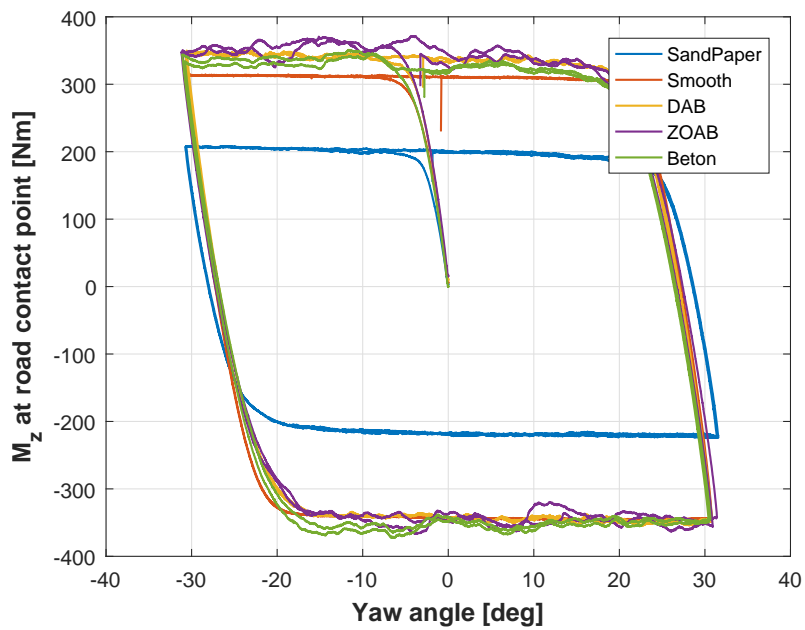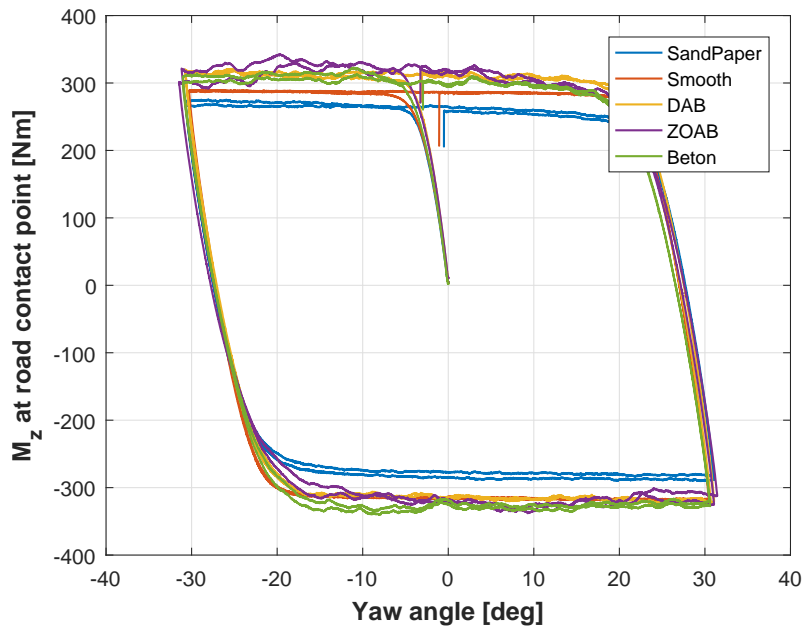

Figure A.21: Tyre 3 M_z vs ψ (Inflation pressure: 180 kPa, Vertical force: 5500 N)

Figure A.22: Tyre 3 M_z vs ψ (Inflation pressure: 210 kPa, Vertical force: 3500 N)

Figure A.23: Tyre 3 M_z vs ψ (Inflation pressure: 210 kPa, Vertical force: 4500 N)

Figure A.24: Tyre 3 M_z vs ψ (Inflation pressure: 210 kPa, Vertical force: 5500 N)
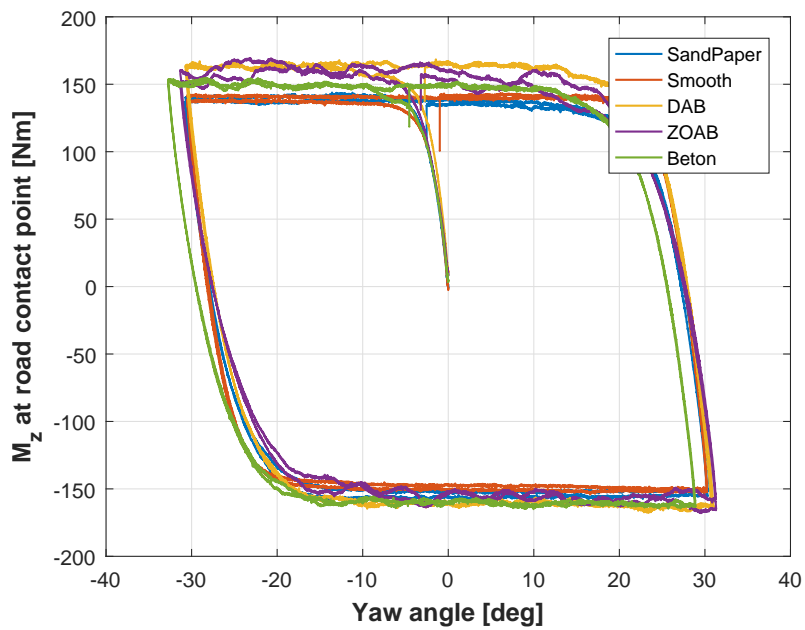

Figure A.25: Tyre 3 M_z vs ψ (Inflation pressure: 240 kPa, Vertical force: 3500 N)
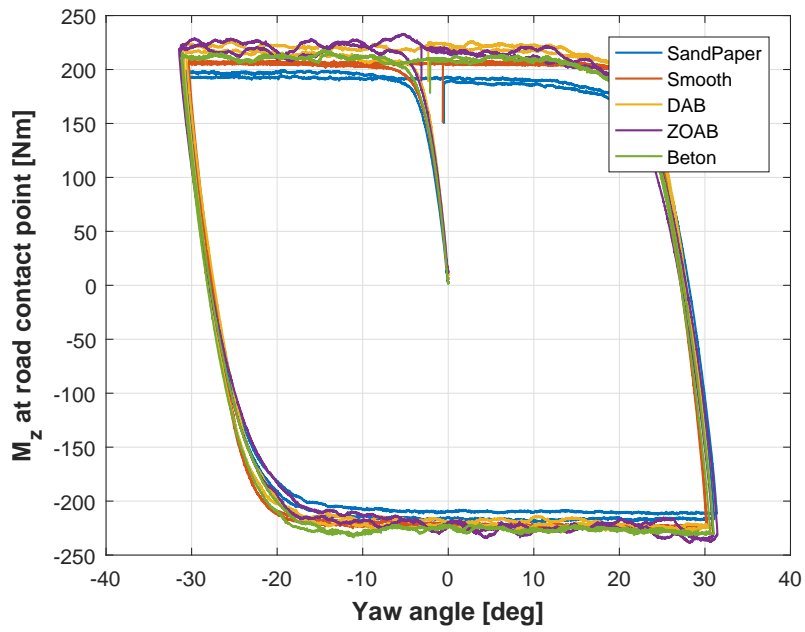
Figure A.26: Tyre 3 M_z vs ψ (Inflation pressure: 240 kPa, Vertical force: 4500 N)
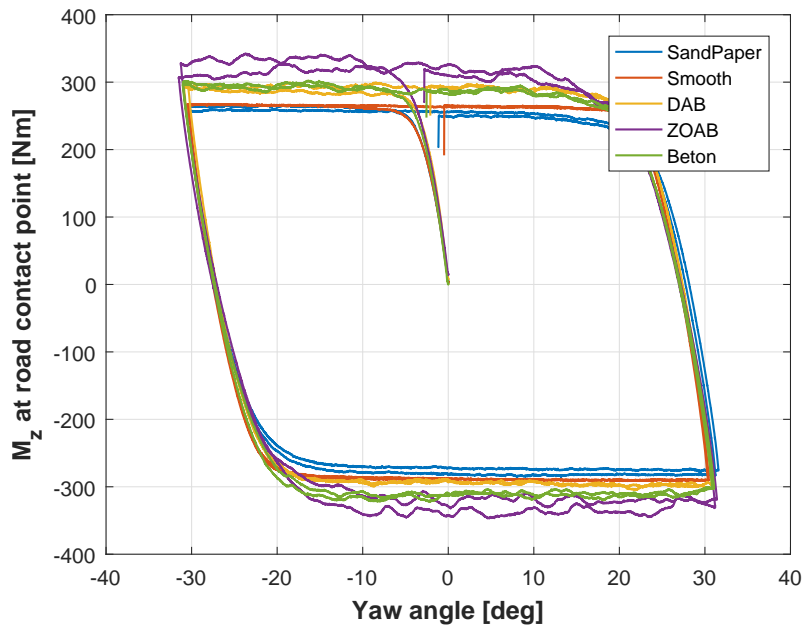

Figure A.27: Tyre 3 M_z vs ψ (Inflation pressure: 240 kPa, Vertical force: 5500 N)

Influence of different road surface types on tyre turn slip & friction characteristics